Influences on the Emissions of Bacterial Plasmas Generated through Nanosecond Laser-Induced Breakdown Spectroscopy

By

Dylan J. Malenfant

A Thesis
Submitted to the Faculty of Graduate Studies
through the Department of Physics
in Partial Fulfillment of the Requirements for
the Degree of Master of Science
at the University of Windsor

Windsor, Ontario, Canada

2016

Influences on the Emissions of Bacterial Plasmas Generated through Nanosecond Laser-Induced Breakdown Spectroscopy

By

Dylan J. Malenfant

APPROVED BY:

_____

Dr. A. V. Hubberstey
Department of Biological Sciences

_____

Dr. J. W. McConkey
Department of Physics

_____

Dr. S. J. Rehse, Advisor
Department of Physics

August 2, 2016

Declaration of Co-Authorship / Previous Publication

I. Co-Authorship Declaration

I hereby declare that this thesis incorporates material that is result of joint research, as follows:

This thesis incorporates works that were the outcome of joint research in collaboration with Derek J. Gillies under the supervision of Dr Steven J. Rehse. This collaboration provided the basis for chapters 5 and 8 of the thesis. The key ideas discussed in this thesis are primarily the work of the author, and the contributions of the co-author were primarily in the act of data acquisition as well as the discussion and refinement of the ideas taken from the results of those studies.

I am aware of the University of Windsor Senate Policy on Authorship and I certify that I have properly acknowledged the contribution of other researchers to my thesis, and have obtained written permission from each of the co-author(s) to include the above material(s) in my thesis.

I certify that, with the above qualification, this thesis, and the research to which it refers, is the product of my own work.

II. Declaration of Previous Publication

This thesis includes one original papers that have been previously published/submitted for publication in peer reviewed journals, as follows:

Thesis Chapter	Publication title/full citation	Publication status*
Chapters 5 and 8	D.J. Malenfant, D.J. Gillies, and S.J. Rehse, Appl. Spectrosc., **70** (3), 485 (2016)	*published*

I certify that I have obtained a written permission from the copyright owner(s) to include the above published material(s) in my thesis. I certify that the above material describes work completed during my registration as graduate student at the University of Windsor.

I declare that, to the best of my knowledge, my thesis does not infringe upon anyone's copyright nor violate any proprietary rights and that any ideas, techniques, quotations, or any other material from the work of other people included in my thesis, published or otherwise, are fully acknowledged in accordance with the standard referencing practices. Furthermore, to the extent that I have included copyrighted material that surpasses the bounds of fair dealing within the meaning of the Canada Copyright Act, I certify that I have obtained a written permission from the copyright owner(s) to include such material(s) in my thesis.

I declare that this is a true copy of my thesis, including any final revisions, as approved by my thesis committee and the Graduate Studies office, and that this thesis has not been submitted for a higher degree to any other University or Institution.

Abstract

In the past decade, laser-induced breakdown spectroscopy has been shown to provide compositional data that can be used for discrimination between bacterial specimens at the strain level. This work demonstrates the viability of this technique in a clinical setting. Studies were conducted to investigate the impact of emissions generated by a nitrocellulose filter paper background on the classification of four species: *E. coli*, *S. epidermidis*, *M. smegmatis*, and *P. aeruginosa*. Limits of detection were determined as 48±12 kCFU per ablation event for new mounting procedures using standard diagnostic laboratory techniques, and a device for centrifuge filtration was designed for sampling from low-titer bacterial suspensions. Plasma emissions from samples grown at biological levels of magnesium, zinc, and glucose were shown not to deviate from controls. A limit of detection for environmental zinc was found to be 11 ppm. Discrimination with heat-killed samples was demonstrated, providing a sterile diagnostic environment.

Acknowledgements

First and foremost, I must thank my advisor, Dr Steven J. Rehse, who offered me this position in his laboratory and whose advice and guidance made this work possible. By extension, I need to acknowledge the efforts of my lab group as a whole and their contributions towards this project: Derek J. Gillies and Russell Allen Putnam, who were instrumental in teaching me the ins and outs of these experiments when I first started; Siddharth Doshi, whose microbiological insights were integral to the work of chapter 7; Allie Paulick and Justine Cunningham, who helped to characterize the centrifuge insert; Vlora Riberdy and Alex Chesnik, who provided sounding boards for my frustrations and solutions to half of those; and Anthony Piazza, who set up the spreadsheet for RM3. Thank you all for keeping me sane when things went off the rails.

Thank you to my family, particularly my parents, and my fiancée, Courtney, for their patience whenever I tried to explain what went wrong in the lab. Your support is what made all of this possible. I apologize that it won't stop any time soon.

Now the bulk list. Thank you to all the friends who supported me. Without a place to go where I could let go of the lab, I wouldn't have made it through this, so thank you Miki, Sean, Keith, Tina, Pat, Andy, Cam, Garnet, Alex, Kaylyn, Kelly, Kayla, Cassandra, Katy, Eric, and Andrew. I'm sure I missed people, but you'll forgive me.

My name may be on this book, but I am far from the only one who contributed to it.

Table of Contents

List of Tables

List of Figures

Chapter 1: Introduction

1.1 Motivation

Over the last 15 years, it has been established that laser-induced breakdown spectroscopy (LIBS) can be used to identify and distinguish bacterial pathogens.[1, 2, 3, 4] This result has a great deal of potential significance in many industries, from medical applications to food and environmental safety to security against bioterrorism threats. This technique can be of particular use in medicine, as it has been shown that LIBS can discriminate between strains of the same bacterial species.[4, 5] With the rate of healthcare-acquired methicillin-resistant *Staphylococcus aureus* (MRSA) infection on the rise, increasing 1000% from 1995 to 2009, the need for a rapid and accurate diagnostic for bacterial infection is greater than ever.[6] By providing a means to healthcare providers to quickly and accurately identify bacterial pathogens, more targeted treatment can be administered in place of the broad-spectrum antibiotics that have given rise to these antibiotic-resistant strains.

While all have had similar implementations in mind, experiments to date have largely been performed in a laboratory environment dissimilar to that in which these tests would normally be of use. In this work, my aim was to first establish a new mounting protocol for performing LIBS on biological samples that more closely resembles the diagnostic tools currently used by clinicians and secondly begin testing the extremes at which this sampling protocol still functioned in terms of concentration, environmental contamination, and exposure to sterilizing effects such as heat-killing and ultraviolet radiation, defining the limits of its effectiveness.

1.2 Laser-Induced Breakdown Spectroscopy

The primary experimental technique used in this work is laser-induced breakdown spectroscopy (LIBS). LIBS uses a high-energy pulsed laser focused onto some target, in this case, a bacterial lawn, in order to create a weakly-ionized plasma. As the excited atoms and ions relax and recombine to their ground states, photons are generated via spontaneous emission specific to the constituent atoms of the sample. This emission acts

as a relative measure of the atomic content of the sample. The spectra produced by LIBS can then be used to create a "spectral fingerprint" of the ablated material.[3] This technique typically makes use of nano- or femtosecond laser pulses focused using various optics, some method of light collection, and a spectrometer in order to yield reproducible spectra with high signal-to-noise ratios as seen in figure 1.1 which shows the intensity of the optical emission of a LIBS plasma from a bacterial target as a function of wavelength, from 200 to 780 nm. The spectroscopically narrow atomic emission lines exhibit excellent signal to noise. The LIBS technique will be discussed in detail in chapter two.

The speed of this process makes the technique very attractive for the implementations described above. The specific experimental apparatus used for this work will be discussed in chapter three.

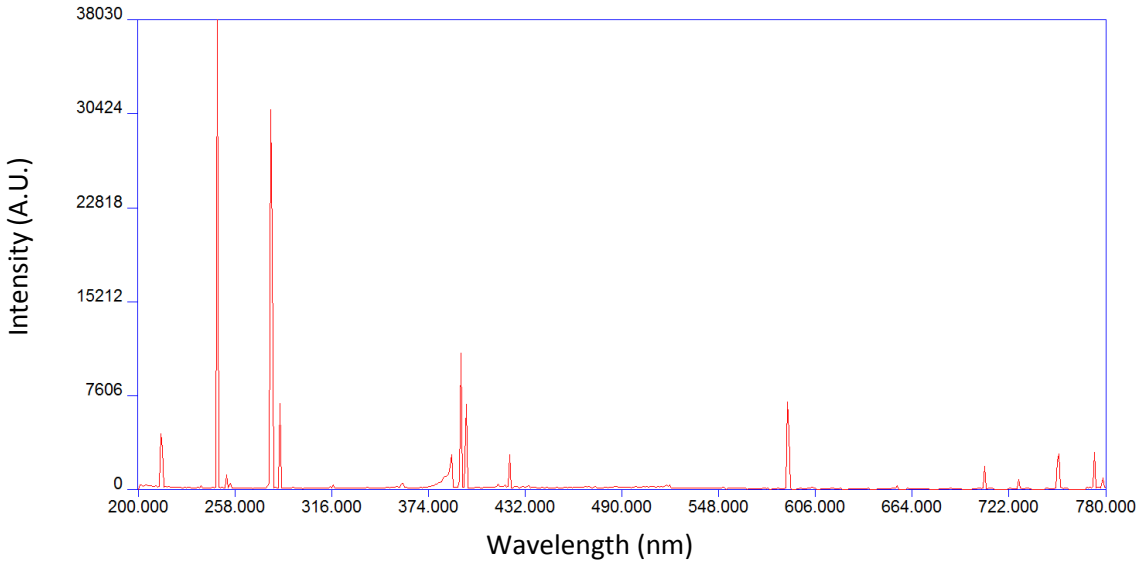

Figure 1.1: LIBS spectrum acquired from an *E. coli* specimen mounted on a nitrocellulose filter

1.3 Current Results for LIBS on Bacterial Samples

Initial work in bacterial identification with LIBS showed the ability to discriminate between bacterial samples, pollens, and molds for the purpose of defense against biological warfare agents.[1] Since then, advancements have been made in the precision of LIBS measurements to the point of differentiating between strains within individual species of bacteria. This was shown in 2007, when Diedrich et al. used a discriminant function analysis algorithm to differentiate between three strains of *E. coli*.[7] These results

were repeated in 2010, when another group showed discrimination between four MRSA strains and one strain of *E. coli* using a projection to latent structures-discriminant analysis (PLS-DA).[4] Most recently, Manzoor et al. showed a discrimination between 40 bacterial strains across three species using a neural network for discrimination. This technique was found to be able to discriminate between strains differing by a single gene with upwards of 95% accuracy.[5] The details of the mathematical algorithms used by others and by me to perform spectral discrimination of bacteria will be discussed in depth in chapter four. A table of all bacterial species that have been the subject of LIBS experiments is provided in table 1.1 at the end of this chapter. Multiple strains of some of the species listed have also been used in experiments, but are not noted in this table.

Studies have also been conducted into the impact of various metabolic stressors on the ability to achieve a successful identification. In 2007, the Rehse group showed that it was possible to discriminate between samples of a single *P. aeruginosa* strain grown on standard trypticase soy agar nutrient media from that grown on a blood agar plate or MacConkey agar.[8] As an extension of this line of inquiry, the group also found that the metabolic state of the bacteria did not have an adverse effect on discrimination when the cells were sterilized via autoclave or inactivated by UV exposure.[9] In 2015, this result was extended, with Sivakumar et al. finding that it was possible to discriminate live and "dead" bacteria killed by autoclaving when using a femtosecond laser for ablation.[10]

1.4 Scope of Thesis

The scope of this work is to characterize the behaviour of LIBS spectra obtained from bacterial samples when ablated on a nitrocellulose filter paper background. I will verify that this technique provides no loss in accuracy relative to our previous methodology as well as demonstrating limits to this new procedure.

In chapter two, I will provide the scientific background necessary for this work. This will include a discussion of laser-induced breakdown for the generation of plasmas used for discrimination and analysis as well as some rudimentary features of bacterial physiology that are relevant to my experiments. In chapter three, I will discuss the apparatus used to collect my data as well as the procedures used to grow and mount

samples. The fourth chapter will provide information on the chemometric techniques used for data analysis. This will include the results of my primary investigation of the new mounting procedure's efficacy. Chapter five will present the results of concentration studies performed using the new mounting procedure in an effort to determine a limit of detection for the apparatus. Chapter six will describe the microcentrifuge insert I designed in an effort to produce a more regular bacterial lawn at low concentrations. I will discuss the characterization of the tool and present a second concentration study performed using the insert. In chapter seven, I will discuss studies performed on bacterial samples grown on media doped with an excess of atomic and molecular species. In chapter eight, studies on the impact of sterilization and inactivation of the bacteria on classification will be discussed. In the ninth and final chapter, I will summarize the results of my work as well as providing recommendations for future work on this project.

Table 1.1: A list of bacterial species investigated in LIBS experiments to date[a]

Species	Author	Year of Publication
Acinetobacter baumannii	Multari	2013
Acinetobacter baylyi	Baudelet	2006
Acinetobacter calcoaceticus	Lewis	2011
Bacillus anthracis	Kiel	2003
	Multari	2012
Bacillus atrophaeous	Morrel	2003
	Hybl	2003
	Samuels	2003
	Leone	2004
	Hahn	2005
	De Lucia	2005
	Gottfried	2007
	Miziolek	2008
	Gottfried	2011
	Cisewski	2012
Bacillus cereus	Samuels	2003
	De Lucia	2005
	Cisewski	2012
Bacillus megaterium	Kim	2004
Bacillus pumilus	Hahn	2005
Bacillus subtilis	Kim	2004
	Baudelet	2006
	Guyon	2006
	Merdes	2007
Bacillus thuringiensis	Morrel	2003
	Kiel	2003
	Samuels	2003
	Leone	2004
	Kim	2004
	De Lucia	2005
	Cisewski	2012
Enterobacter cloacae	Lewis	2011
	Mohaidat[b]	2012
	Putnam[b]	2013
Erwinia chrysanthemi	Baudelet	2006
Escherichia coli	Morrel	2003
	Leone	2004

Species	Author	Year of Publication
Escherichia coli	Kim	2004
	Baudelet	2006
	Guyon	2006
	Rehse[b]	2007
	Rehse[b]	2007
	Rehse[b]	2009
	Rehse[b]	2010
	Multari	2010
	Barnett	2011
	Gottfried	2011
	Marcos-Martinez	2011
	Mohaidat[b]	2011
	Mohaidat[b]	2012
	Multari	2013
	Putnam[b]	2013
	Manzoor	2014
	Sivakumar	2015
	Malenfant[b]	2016
Geobacillus stearothemophilus	Hahn	2005
	Cisewski	2012
Klebsiella pneumoniae	Multari	2013
	Manzoor	2014
Methylophilus methylotrophus	Lewis	2011
Mycobacterium smegmatis	Rehse[b]	2010
	Mohaidat[b]	2011
	Mohaidat[b]	2012
	Putnam[b]	2013
	Malenfant[b]	2016
Pantoea agglomerans	Lewis	2011
Proteus mirabilis	Morrel	2003
	Leone	2004
Pseudomonas aeruginosa	Rehse	2007
	Lewis	2011
	Marcos-Martinez	2011
	Multari	2013
	Manzoor	2014
	Malenfant[b]	2016
Salmoella enterica	Barnett	2011

Species	Author	Year of Publication
Salmonella pullorum	Manzoor	2014
Salmonella salamae	Manzoor	2014
Salmonella typhymurium	Marcos-Martinez	2011
	Manzoor	2014
Shewanella oneidnsis	Baudelet	2006
Staphylococcus aureus	Morrel	2003
	Leone	2004
	Rehse[b]	2010
	Multari	2010
	Barnett	2011
	Mohaidat[b]	2012
	Multari	2013
	Putnam[b]	2013
Staphylococcus epidermidis	Malenfant[b]	2016
Staphylococcus saprophyticus	Rehse[b]	2010
	Mohaidat[b]	2012
	Putnam[b]	2013
Streptococcus mutans	Rehse[b]	2009
	Rehse[b]	2010
	Mohaidat[b]	2012
	Putnam[b]	2013
Streptococcus viridans	Rehse[b]	2010
	Mohaidat[b]	2011
	Mohaidat[b]	2012
	Putnam[b]	2013

[a] Specific strains utilized for experiments are not noted

[b] These studies were performed by the Rehse research group

References

[1] A.C. Samuels *et al.*, Appl. Opt., **42** (30), 6205 (2003)

[2] S. Morrel *et al.*, Appl. Opt., **42** (30), 6184 (2003)

[3] J.D. Hybl, G.A. Lithgow, and S.G. Buckley, Appl. Spectrosc., **57** (10), 1207 (2003)

[4] R.A. Multari *et al.*, Appl. Spectrosc., **64** (7), 750 (2010)

[5] S. Manzoor *et al.*, Talanta, **121**, 65 (2014)

[6] *Healthcare-Associated Infections - Due Diligence*, Public Health Agency of Canada. <http://www.phac-aspc.gc.ca/cphorsphc-respcacsp/2013/infections-eng.php>

[7] J. Diedrich and S.J. Rehse, J. Appl. Phys., **102**, 014702 (2007)

[8] S.J. Rehse, J. Diedrich, and S. Palchaudhuri, Spectrochim. Acta Part B, **62**, 1169 (2007)

[9] Q. Mohaidat, S. Palchaudhuri, and S.J. Rehse, Appl. Spectrosc., **65** (4), 386 (2011)

[10] P. Sivakumar *et al.*, Astrobiol., **15** (2), 144 (2015)

Chapter 2: Experimental Background

2.1 Laser-Induced Breakdown Spectroscopy (LIBS)

In 1960, Theodore Maiman developed a solid-state ruby laser that operated at a wavelength of 694.3 nm. Four years later, the neodymium-doped ytterbium-aluminum-garnet laser (Nd:YAG) that has become so ubiquitous was invented by Geusic, Marcos, and van Uitert. Throughout the 60's and 70's, these lasers were used to perform various experiments involving ablation of materials to generate laser-induced plasmas (LIP) for optical spectroscopy. In the 1980's, this line of experiments was resurrected at Los Alamos National Laboratory as a means for standoff detection of hazardous gases through ablation using a Nd:YAG laser.[1, 2] In 2003, LIBS was used for the identification and detection of bioaerosols and bacteria for the first time.[3, 4, 5]

LIBS is, in its most basic form, a fairly simple procedure. A high pulse energy laser is used for ablation of a target and to generate a LIP. While the Nd:YAG used for the experiments discussed in this thesis is very common, many other models operating at a wide range of wavelengths and pulse durations are used. Since LIBS relies almost exclusively on non-resonant thermal processes, wavelength is generally only a factor with regard to its absorption by the material to be ablated. Light emitted from the plasma is then collected and analyzed using a high-resolution spectrometer with a wide range of wavelength response. This is often achieved with the use of an echelle spectrometer or several spectrometers each corresponding to a different wavelength range.

In this chapter, I will discuss the process of generating the light used for spectroscopy, specifically the plasma formation and some rudimentary dynamics of the plasma. The analysis of the collected light will be touched upon in the next chapter with the discussion of the experimental apparatus.

2.1.1 Plasma Formation

The process for the formation of a plasma via laser ablation varies depending on the pulse duration used. A plasma created using a femtosecond laser is very different from that created by a nanosecond pulse. This discussion will be limited to the nanosecond regime used in my experiments.

A LIP requires a laser pulse of an intensity between 10^8-10^{10} W/cm^2 to be focused onto the target material.[6] LIBS has been used previously for the analysis of gases, solids, liquids, and aerosols. In a solid target, the energy from the pulse will be absorbed through largely thermal processes, heating, melting, and vaporization, resulting in the ablation event which can take place on a timescale from several to tens of nanoseconds. Debris from the ablation will be thrown up from the newly formed crater and begin absorbing energy from the laser. Ionization will occur first through multi-photon ionization events causing the plasma ignition, and the freed electrons will be heated via inverse bremsstrahlung. This results in a cascade of ionization events as the accelerated electrons free others through impact ionization. These effects result in the shielding of the substrate from additional laser energy once a critical electron density is achieved.[6] The plasma is typically weakly ionized (<10% ionization) and in general contains only atomic and ion species. This process occurs over the duration of the laser pulse, in our case, 8 ns. This process is shown schematically in Figure 2.1.

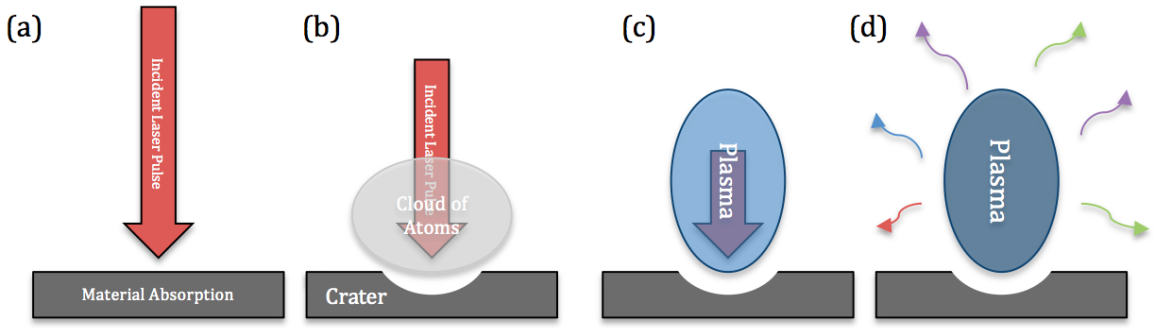

Figure 2.1: Schematic of the laser ablation leading to LIP formation. (a) A high-energy laser pulse is incident on the target and absorbed through mostly thermal processes. This results in (b) vaporization of a cloud of atoms and molecular fragments above the target, which then absorbs remaining laser light. (c) The absorption of energy from the laser pulse ionizes the atoms in the cloud, resulting in the formation of the plasma. (d) As the plasma cools, spontaneous emission of photons occurs. These photons are collected for analysis

In vacuum, a LIP will expand adiabatically. Heat will neither enter nor leave the plasma plume. When the plasma is created in a gaseous environment, shockwaves are formed as the plasma plume expands into its surroundings. The ambient medium does work on the plasma as this happens which increases the plasma temperature and electron

density.[7, 8] This effect is illustrated in the following figures from Unnikrishnan *et al*. In this work, argon was chosen for an ambient medium for plasma formation. This is because the

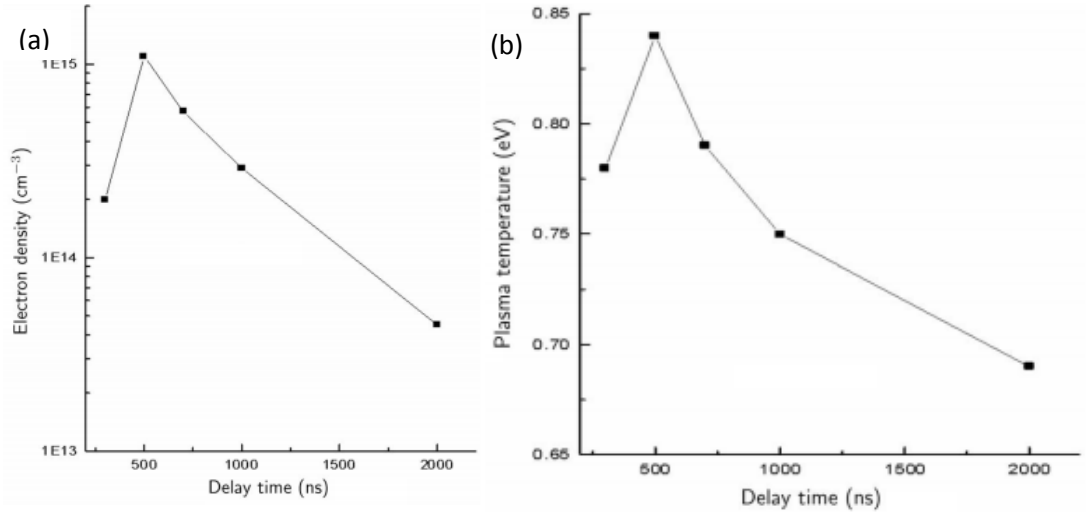

Figure 2.2: Plots of (a) electron density and (b) plasma temperature for LIBS plasmas generated from a copper target as a function of time. Plasmas were observed for a 750 ns window starting at the indicated delay time after the initial laser pulse[9]

increase in temperature and electron density are correlated to the mass of the ambient gas particles, and argon provides a massive gas while also providing little contribution to the observed spectra.[8] This expansion continues until the plasma pressure equilibrates with the external environment, typically on the order of tens of microseconds after plasma ignition. The increased plasma temperature results in a greater population in the higher energy states of the constituent species of the plasma, resulting in more emission from the transitions from these states.

For the first several hundred nanoseconds after plasma formation, plasma emission is dominated by broadband radiation caused by bremsstrahlung and recombination of free electrons with ions in the plasma. During this time, free electron density is typically at its highest. It is integral to LIBS that a high electron density be achieved during this period as free electron interactions are responsible for all observed emissions. Excited species are formed through free-bound recombination events as well as collisional excitation of the species present in the plasma.[6, 7, 10] Emission from ions is also observed strongly in the nanosecond regime, though Stark effects are particularly strong at this time.[7] As a result of the strong non-specific background emissions which

dominate at early times after plasma ignition, plasma observation must be delayed in time. Shortly after plasma formation (starting around 1 μs) the plasma begins cooling, and atomic emission begins to dominate.[7] Some molecular emission can typically be observed as the plasma temperature decreases and species in the plasma begin to recombine. Emission from C_2 (the C-C Swan band) and molecular CN are both commonly observed in bacterial spectra and were seen in this work. An example of molecular emission due to the presence of CN molecules is shown in Figure 2.3. These molecular species are formed in the plasma after ablation and are not indicative of bonds in the ablated target itself.[11] These emissions are generally collected via an optical fibre coupled to the spectroscopic system.

2.1.2 Plasma Characteristics

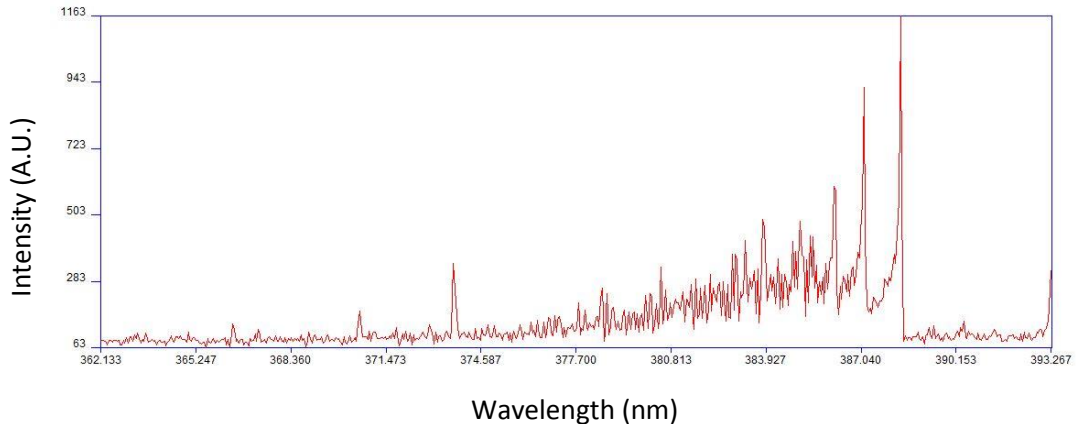

Figure 2.3: A molecular CN band as observed in spectra acquired from *S. epidermidis*

Typically, the temperature of a plasma in local thermodynamic equilibrium, one in which the temperature of the free electrons and the ions and atoms are equal, as well as the free electron density are reported as a means of characterization of the plasma. The temperature of the plasma can most simply be determined experimentally by creating a so-called Boltzmann plot. The Boltzmann plot makes use of the relationship

$$I_{jk} = \frac{hc}{4\pi\lambda_{jk}} A_{jk} \lambda_D \frac{N}{Z} g_k e^{-\frac{E_k}{k_B T}} \qquad (1)$$

where I_{jk} gives the emission intensity of the transition from levels *k* to *j*, λ_{jk} is the wavelength of the photon emitted in this transition, A_{jk} is the Einstein *A* coefficient for

the transition, and g_k, Z, and E_k are the multiplicity, partition function, and energy of the upper energy level. λ_D and N are properties of the plasma, namely the Debye length of the plasma and number density of atoms in the ionization state for the *j*-*k* transition. By taking the natural logarithm of this relationship, we can see that

$$\ln {I_{jk}}' = -\frac{1}{k_B T} E_k + C \qquad (2)$$

where ${I_{jk}}'$ is the intensity scaled by the factor $\frac{hc}{4\pi\lambda_{jk}} A_{jk} \lambda_D \frac{N}{Z} g_k$ and C is a constant. By plotting the rescaled intensity of many emission lines (or at least several, although more is preferable) as a function of their respective upper energy levels, E_k, a linear plot with a slope of $-\frac{1}{k_B T}$ can be generated.[9]

The electron density of a plasma can be estimated through either Stark broadening effects or the Saha-Boltzmann equation. The full width at half-maximum of a Stark-broadened emission line is given by

$$\Delta\lambda_{1/2} = 2W\left(\frac{N_e}{10^{16}}\left(1 + 1.75A\left(\frac{N_e}{10^{16}}\right)^{1/4}\right)\left(1 - \frac{3}{4}\,{N_D}^{-1/3}\right)\right) \qquad (3)$$

$$N_D = 1.72 \times 10^9 \frac{{T_e}^{3/2}}{{N_e}^{1/2}} \qquad (4)$$

where W and A are electron and ion impact parameters that are obtained from reference materials, N_e is the electron density, N_D gives the number of particles in the Debye radius and is estimated based on the electron temperature, T_e, and number density, N_e, and $\Delta\lambda_{1/2}$ is the FWHM of the broadened line.[7] This technique is particularly useful with hydrogen emission lines and lines from hydrogen-like atoms which demonstrate Stark broadening many times larger than the linewidth of typical spectrometers for the electron density typical in LIPs.

Alternatively, the Saha-Boltzmann equation yields

$$N_e = \frac{{I_0}^*}{{I_1}^*} 6.04 \times 10^{21} T^{3/2} e^{\frac{-E_{k,1} + E_{j,0} - E_\infty}{k_B T}} \qquad (5)$$

where $I^* = \frac{I\lambda}{gA}$ is a modified intensity of emission lines from two subsequent ionization states (in this case the neutral state denoted by subscript 0 and the first or singly-ionized state denoted by subscript 1,) and E_∞ gives the ionization energy of the lower of the two states.[9]

Unfortunately these methods are not applicable to this work due to the nature of the spectra involved. The Saha-Boltzmann relation shown in equation 5 requires the use of a neutral and ion emission line from the same atomic species. Very few of these are available in bacterial spectra, and of those that do exist, too much variation exists in the neutral lines to make for a reliable measure. Were more ion-neutral pairs available, an average value could be used to overcome this variation, but the data does not allow for this. A Boltzmann plot, likewise, requires many lines from a single atomic species over a wide range of upper energy levels. Without this, the calculated slope cannot be claimed to have any useful information. This precludes its use in the bacterial spectra I collect, where there not enough lines to validate such a calculation. Without one or the other of the above methods to calculate an electron temperature or density, Stark methods cannot be used to calculate the remaining parameter.

2.2 Bacterial Physiology

Due to the high temperatures of the LIP, the initial structure of a bacterial cell is destroyed during ablation. In general, molecular bonds are not preserved during nanosecond ablation.[7] While the structures may no longer exist, it has been shown that LIBS bacterial emission is strongly tied to the composition of the cellular wall.[12] For this reason, I will provide a brief overview of membrane physiology. This will cover three general categories that are represented by the species chosen for the following experiments, Gram positive, Gram negative, and acid-fast. These categories are defined by the bacterium's response to the Gram staining procedure in which the cells are stained with a dye called crystal violet, modified with potassium iodide, and washed with alcohol.[13] Results obtained by Baudelet in 2006 using a method called trace element hyperspace classification (TEHC) showed a separation of bacterial groups strongly corresponding to these cell wall properties.[14]

2.2.1 Gram Positive

A Gram positive bacterium is one that is dyed purple during the Gram procedure. The cell wall of these species is made up of a complex polymer called peptidoglycan or murein. Murein contains alternating units of N-acetyl glucosamine and N-acetyl muramic acid. Its muramic acid components are in turn bonded to a peptide. This molecule is shown in Figure 2.4.These peptides may link to each other across strands of murein, resulting in a two-dimensional structure.[13] Because of the sugars and charged amino acids, murein creates a layered, dense hydrophilic barrier around the cell. It is this layer that retains the crystal violet dye during the staining process.

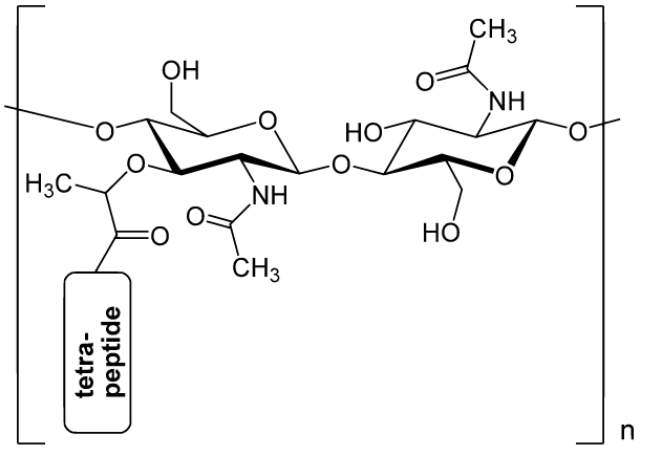

Figure 2.4: Chemical structure of murein

Aside from acting as a barrier to potentially hazardous hydrophobic chemicals such as bile salts, murein acts as a structural reinforcement to the cell, providing a rigid structure that prevents cell lysis from pressure differential across the cell membrane. When this layer is dissolved, the cell becomes a spheroplast if it is in an environment of approximately osmotic pressure. The lack of a murein corset causes the cell to take on a spherical shape to best distribute pressure and prevent lysis.[13] In this work, *Staphylococcus epidermidis* was used as a representative Gram positive species.

2.2.2 Gram Negative

After the alcohol washing step in a Gram stain, a counter stain called safranin is added. This dye turns Gram negative cells pink. These cells use a double membrane structure than sandwiches a much thinner (relative to Gram positive species) murein wall.

The outer membrane is not only chemically distinct from the inner membrane but also contains a compound that is completely unique to these bacteria.[13] The bilayered membrane's outer layer is made up of bacterial lipopolysaccharides (LPS). LPS has a phosphorylated disaccharide to which fatty acids attach. This compound, called lipid A, faces the inside of the bilayer, much like the usual phospholipid bilayer structure of animal cells. This is bound to a short series of sugars called the core polysaccharide that is fairly uniform across most Gram negative species. In turn, these sugars are attached to a repeating chain of O antigen subunits that exclude hydrophobic compounds from entering the cell.[13] This compound is part of why these bacteria can be so dangerous. Lipid A, also known as endotoxin, can cause fever in a host organism, and in large doses, it can also cause shock and death.[13] As its name would imply, the O antigen is also highly antigenic.

While LPS provides a necessary protection from hydrophobic chemicals, the lipid bilayer also works to the exclusion of hydrophilic species necessary for the cell's survival. For this reason, the membrane is also peppered with microchannels called porins to allow the passive diffusion of smaller hydrophilic chemicals. Any chemicals large than a porin (600-700 daltons) would typically (pass through the membrane via specific transport mechanisms.[13]

Between the outer and inner membrane of the Gram negative cells exists a space called the periplasm. The periplasm contains the murein cell wall as well as degradative enzymes to break down larger molecules to be brought into the cytoplasm and enzymes called β-lactamases that inactivate certain antibiotics such as penicillins and cepalosporins.[13, 15] This region also contains binding proteins that aid in the collection of sugars and amino acids from the medium in which the cell grows. Both *Escherichia coli* and *Pseudomonas aeruginosa* were used in this work as representative Gram negative bacteria.

2.2.3 Acid-Fast Bacteria

Acid-fast bacteria are notable for having an irregular response to dye stains. Should a dye be introduced to the cell, it cannot be removed by application of dilute hydrochloric acid, hence the name acid-fast or acid-resistant bacteria.[13] These cells

contain complex hydrocarbon chains called waxes interlaced throughout their murein cell wall. While their waxy coating acts as a protective layer against harsh chemicals in the environment, it also provides a limit to nutrient uptake. As a result, they tend to grow and divide very slowly.[13] *Mycobacterium smegmatis* was used as an example of acid-fast bacteria in these studies.

References

[1] L.J. Radziemski and T.R. Loree, Chem. Plasma Process, **1** (3), 281 (1981)

[2] L.J. Radziemski *et al.*, Anal. Chem., **55** (8), 1246 (1983)

[3] A.C. Samuels *et al.*, Appl. Opt., **42** (30), 6205 (2003)

[4] S. Morrel *et al.*, Appl. Opt., **42** (30), 6184 (2003)

[5] J.D. Hybl, G.A. Lithgow, and S.G. Buckley, Appl. Spectrosc., **57** (10), 1207 (2003)

[6] D.A. Cremers and L.J. Radziemski, *Handbook of Laser-Induced Breakdown Spectroscopy*, 1st Ed. (West Sussex, England, 2006)

[7] J.P. Singh and S.N. Thakur, *Laser-Induced Breakdown Spectroscopy*, 1st Ed. (Amsterdam, The Netherlands, 2007)

[8] M. Dawood, Ph.D. thesis, Université de Montréal

[9] V.K. Unnikrishnan *et al.*, Pramana, **74** (6), 983 (2010)

[10] J. Cooper, Rep. Prog. Phys., **29** (1), 35 (1966)

[11] M. Baudelet *et al.*, Appl. Phys. Lett., **88**, 063901 (2006)

[12] S.J. Rehse *et al.*, J. Appl. Phys., **105**, 102034 (2009)

[13] M. Schaechter *et al.*, *Mechanisms of Microbial Disease*, 3rd Ed. (Baltimore, USA, 1999)

[14] M. Baudelet *et al.*, Appl. Phys. Lett., **89**, 163903 (2006)

[15] K. Bush, G.A. Anthony, A.A. Medeiros, Antimicrobial Agents Chemotherapy, **39** (6), 1211 (1995)

Chapter 3: Apparatus and Methodologies

3.1 LIBS Apparatus

Laser-induced breakdown spectroscopy requires three major elements: a laser source and beam-focusing optics to create the plasma, some form of light collection apparatus to collect optical emission from the plasma, and a way of dispersing the light to observe only specific emission wavelengths from the plasma (i.e. a monochromator, a spectrometer, or notch filters). The apparatus used for this work was initially assembled at Wayne State University. It was disassembled and moved to the University of Windsor and reassembled as follows. The laser source used for my experiments was a Quanta Ray Nd:YAG (Spectra Physics LAB-150-10) operating at its fundamental wavelength of 1064 nm with a 10 Hz repetition rate and an 8 ns pulse duration. The laser had an initial pulse energy of approximately 650 mJ per pulse. Pulse energy was reduced to 180 mJ per pulse by using a half-wave plate to rotate the polarization of the beam, then using a polarizing beam splitter (Glan-Taylor calcite polarizer) to discard a portion of the beam into a beam dump. This energy was selected to ensure an energy of approximately 5 mJ per pulse was ultimately incident on the target after the beam passed through a mode-cleaning telescope. High damage threshold 1064 nm high-reflection dielectric-coated mirrors were used to direct the beam to a 3× beam expanding telescope followed by a 9 mm iris for cleaning of the Nd:YAG's quasi-Gaussian spatial mode. This mode cleaner consisted of an anti-reflection (AR) coated planoconcave lens (f=-5 cm, ϕ=2.54 cm) followed by a planoconvex lens (f=18.5 cm, ϕ=7.62 cm) at a distance of 13.5 cm. Another dielectric mirror was used to direct the laser pulse down toward the target. This optical train is shown in Figure 3.1 below. The laser light was then focused onto the target by a 5× AR-coated microscope objective with a long working distance. A beam splitter was placed in the beam line just before the objective in order to allow for visualization of the target with a camera from above. The camera image was displayed on a monitor in order to better visualize the target surface to ensure no location was sampled by the laser multiple times.

The ablation target was mounted on a magnetic pedestal in a Plexiglas box that acted as a purge chamber. This chamber was in turn mounted on an xyz-translation stage.

During data acquisition, the chamber was flushed with argon at a flow rate of 20 SCFH. In order to place the target in the focus of the laser, a HeNe laser was shone into the purge

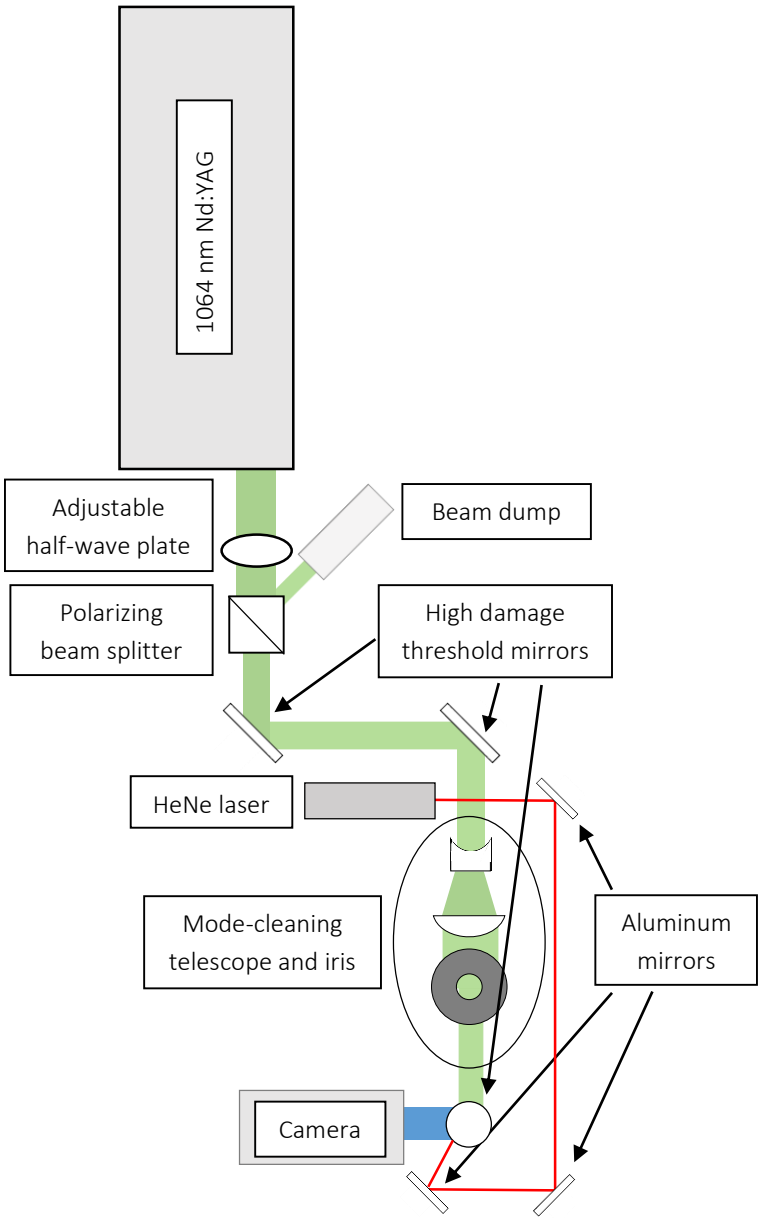

Figure 3.1: Schematic of the optical train used to direct laser pulses to the ablation target

chamber at an angle. As the translation stage was moved along the z-axis, changing the height of the target, the spot created by the HeNe moved across the surface of the target. When the height at which the best ablation occurred was found, a mark was made on the monitor at the location of the HeNe spot. This is illustrated in figure 3.2. For our purposes,

"best" was defined as the height at which the highest intensity of lines of interest were achieved reproducibly after significant experimental optimization.

After ablation, emission was collected by matched off-axis parabolic reflectors (f=5.08 cm, ϕ=3.81 cm) that focused the light into a 1 m steel-encased multimodal optical fibre (core ϕ=600 µm, numerical aperture (NA)=0.22). Many experiments collect light through simply exposing the end of the optical fibre to the plasma, sometimes using a

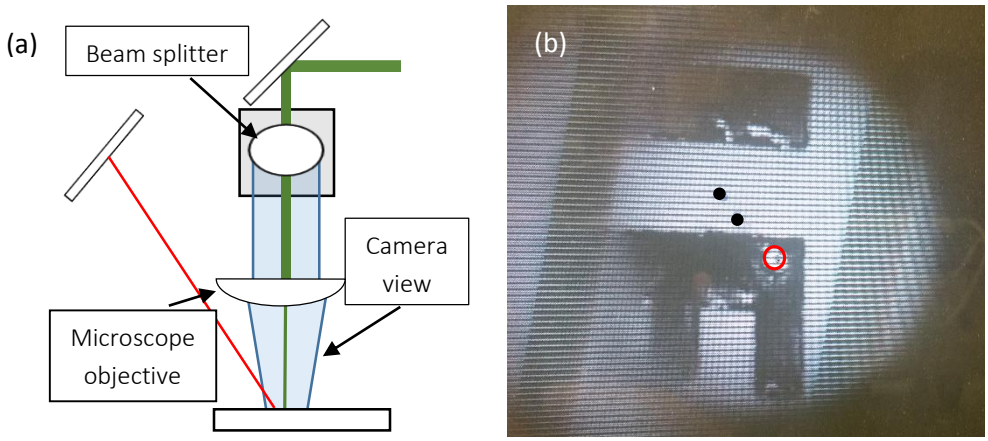

Figure 3.2: (a) Schematic of the focusing and alignment system. (b) View of the target and alignment laser through the camera. Marks drawn on the screen give locations of focus for various targets (marks and laser exaggerated for the figure)

focusing lens.[1-5] Use of these parabolic reflectors increased the amount of light collected, but it also increased the height dependence of the measurements. It is important to ensure that light is being sampled from the same location in the plasma with each laser pulse. Light from the plasma was then dispersed by an échelle spectrometer (ESA 3000, LLA Instruments, Inc.) with spectral resolution from 200 to 800 nm and detected by an intensified CCD camera (Kodak KAF 1001).

3.1.1 Échelle Spectrometer

An échelle spectrometer is one that makes use of an échelle grating to diffract incoming light. The échelle grating is a step-like grating with widely spaced grooves that spreads light into overlapping orders. As the diffraction order increases, the angular spacing for a given wavelength decreases in accordance with the diffraction equation,

$$d[\sin(\theta_i + \theta_B) + \sin(\theta_m + \theta_B)] = m\lambda \quad (1)$$

where θ_i gives the incident angle of the light and θ_m gives the diffracted angle of light at wavelength lambda of order m. θ_B is a parameter called the blazing angle that defines a rotation of the grating such that light is not incident directly on its face, but rather on the flat, step-like face of the groove. The groove spacing of the grating is given by d. It is clear from this equation that, for polychromatic light, different wavelengths of varied order will overlap in a given location. For instance, the same point will be occupied by the first order of 600 nm light, the second order of 300 nm, and the third order of 200 nm. This becomes more exaggerated for higher orders. An échelle spectrometer makes use of this by using a high blazing angle to overlap many wavelengths of high order into a single location, then using a simple prism mounted perpendicularly to the diffraction grating in order to spread the light out into a two-dimensional array. This spreading of wavelength across orders results in a high resolution while still maintaining a wide spectral bandwidth.[6] This dispersion is not uniform across all wavelength, and in the case of the spectrometer used for this work, resolution was maximized in the ultraviolet region of the spectra. The linear

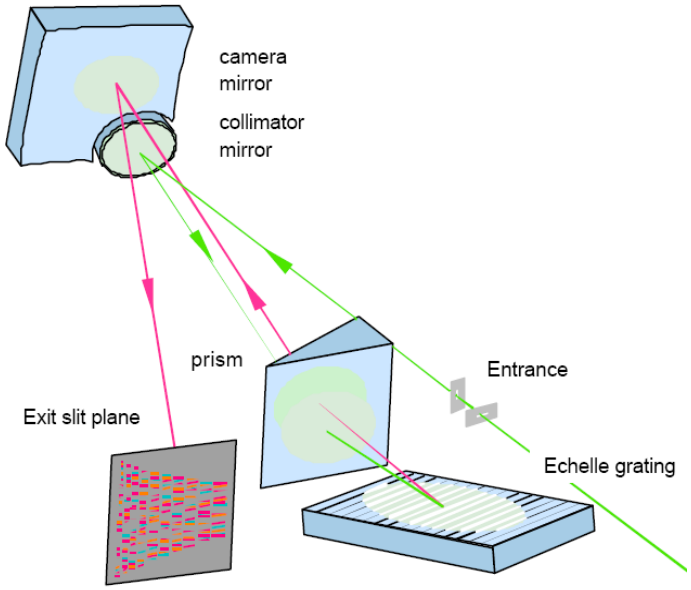

Figure 3.3: Schematic of the cross-dispersion internal optics of the ESA 3000 spectrometer[7]

dispersion per pixel in the UV region was approximately 5 pm per pixel, increasing to 20 pm per pixel in the infrared. This results in a spectral resolution of 30 pm in the UV regions and 120 pm in the infrared.

Once it is dispersed, the light in our echelle spectrometer is imaged onto an intensified charge-coupled device (ICCD) with a one-inch x one-inch chip (1024 x 1024 pixels). A CCD functions via photons generating electron-hole pairs in a grid of potential well capacitors. The number of holes in a given capacitor is then proportional to the intensity of light incident on a given capacitor. The charge of each cell in the grid is then determined by read-out circuits.[7] Locations in this grid are permanently calibrated to certain wavelengths of light according to the diffraction of the grating and prism, as these spectrometers contain no moving parts. This is illustrated in the échellogram shown in Figure 3.4 below which shows the dispersed spectrum from a broadband deuterium tungsten lamp (a) and LIBS emission from a piece of steel (b). This false-colour map indicates charge stored across the orders of the CCD array. In this false colour map, yellow indicates no light and darker colors (purple to black) indicate more light. The green circle

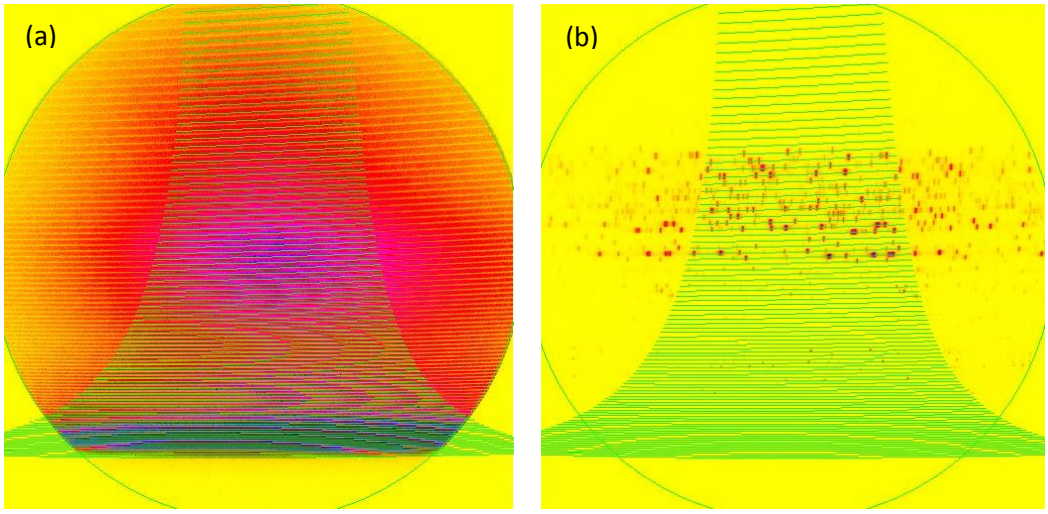

Figure 3.4: Échellograms for (a) a deuterium tungsten broadband source showing the mapping of the incoming light to the CCD chip and (b) the emissions collected from a plasma formed from a steel piece

indicates the image of the dispersed light on the CCD chip. No light is imaged outside of this region. The wavelength of the light dispersed by the spectrometer is then mapped to these locations on the CCD. The pattern indicated by the green horizontal lines represents the orders of the dispersion of light from which our data is taken. Order 119, which contains dispersed light from 200.923 to 202.590 nm, is mapped to the top of the chip and order 29, which contains dispersed light from 820.0439 nm to 835.201 nm, is mapped

to the bottom of the chip. In mapping the dispersion to the image, some information is lost where higher wavelengths in the diffraction pattern fall outside the imaged region. This is shown in figure 3.4 where the horizontal lines fall outside the circle. This loss of some information was allowed to maximize resolution in the ultraviolet region of the spectrum which is mapped to the top half of the CCD chip in Figure 3.4 where many of the lines relevant to this work are found.

To amplify the LIBS emission, the CCD is preceded by a microchannel plate (MCP) image intensifier. When a photon is incident on the MCP, it generates a photoelectron. Voltage applied across the MCP creates an electron cascade that is then incident on a phosphor prior to the CCD creating a shower of monochromatic photons where the number of photons is proportional to the initial photon count. The voltage across the MCP then serves two purposes. First, it acts as an amplification of the initial light incident on the ICCD. This is the trade-off made with the generation of a photon shower from the phosphor screen. A more intense signal is created at the loss of some resolution. As not enough light is collected without amplification to measure a discernable signal, and the resolution loss is minimal, this is more than acceptable. The second use is as a gating mechanism. When no voltage is applied, no signal is received. This allows for nanosecond-timing control of when and for how long a spectrum is collected. The time between a laser pulse and the collection of light is called the gate delay (τ_d), and the time over which a spectrum is collected is called the gate window (τ_w).

3.1.2 Steel Calibration

In order to provide a nominal standard for performance and reproducibility, steel spectra were acquired each day prior to regular data collection. A polished steel calibration target was mounted in the argon purge chamber, and spectra were taken with observation timing τ_d=1 μs and τ_w=10 μs. Each spectrum was acquired after two "clean pulses," two laser pulses meant to ablate any debris that may be on the surface. Each pulse is sufficiently separated in time that there is no overlap between the plasma of the previous pulse with the following laser pulse. Since the steel is nominally unchanging over weeks and months, this gives an idea of the best-case scenario of the functioning and

reproducibility of the system. Data was collected from 65 lines from FeI and FeII. The intensities of these lines was calculated by the spectrometer software (ESAWIN v3.20). For each peak, a region of 60 pixels about the peak wavelength (30 on either side) is taken. The ESAWIN software then determines a background line across this region. A peak search is performed, and if the location of the peak is not within three pixels of the expected wavelength, it is flagged as an error. Otherwise, a full width at half maximum for the peak is determined, and intensity is then defined as the background-subtracted integral over the FWHM.[8] This is shown below in Figure 3.5 which shows a "region of interest," or ROI,

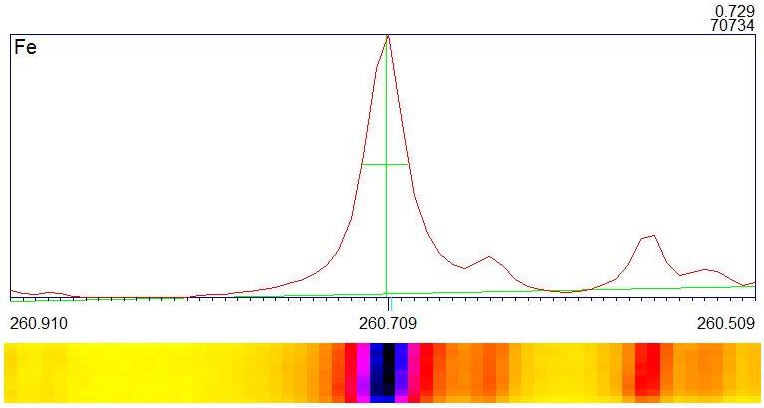

Figure 3.5: ROI view from the ESAWIN software. Green lines designate the background, central wavelength of the emission line, and FWHM. Below the peak, the intensity map from the CCD can be seen. Each wavelength is given the intensity of the average pixel in a column of height *h* along a diffraction order where *h* is a wavelength-dependent parameter. At this wavelength, it can be seen that *h* is six pixels[8]

of 30 pixels on either side of a known iron emission line at 260.709 nm.

Data was recorded for these so-called "raw" intensities (in arbitrary units) over the course of months and years as well as a normalized intensity. Normalized intensities scale the intensity of the measured lines to the sum of the intensities of all measured lines in the spectrum. This is done to account for shot-to-shot stochastic variations in the plasma which can cause a variation in the amount of ablated material or the ablation temperature, both of which (to first order) effect all the lines the same. Based on data collected from April 2014 to July 2016, we measure a shot to shot standard deviation of the normalized intensity on the most intense lines of approximately 5%. The deviation on smaller lines was larger, ranging from 20-25%. This was expected, as the same amount of

noise makes up a larger fraction of the signal in this case. This is shown in figure 3.6 which shows the experimentally determined fractional standard deviation of dozens of lines as a function of their absolute unnormalized intensity. These values give a target to reach for "reproducible" data. In addition, the location of hundreds of known iron emission

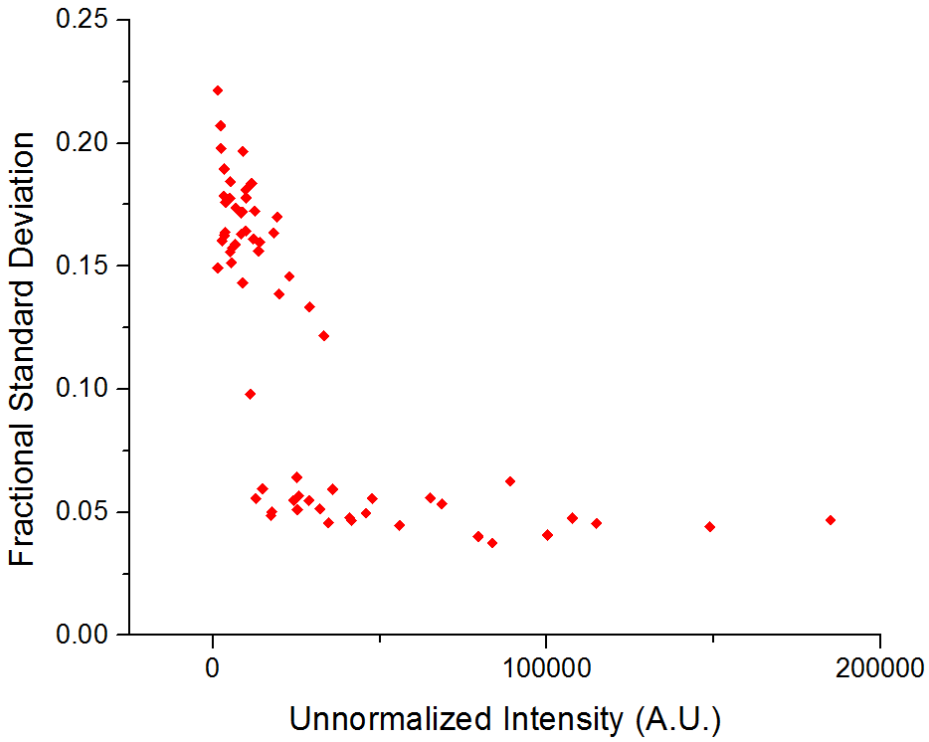

Figure 3.6: Plot of fractional standard deviation as a function of line emission intensity. Based on two years of accumulated data, strong emission lines are expected to vary by less than 10% while weaker lines may vary by up to 25% in a clean, smooth target

lines allowed easy day to day spectral calibration of the spectrometer. As this calibration was performed every time date was collected, it also allowed us to determine when something was not working as expected before any bacterial data was collected.

3.2 Bacterial Sample Preparation

All bacterial samples were provided initially as colonies on an agar plate by Ms Ingrid Churchill of the Biology department at the University of Windsor. In this section, I will discuss the procedures used to maintain the bacterial stock for my experiments and how samples were prepared for experiments.

3.2.1 Media Preparation

All specimens used for experiments were grown on tryptic soy agar (TSA) nutrient media. TSA contains a pancreatic digest of casein, soybean meal, NaCl, dextrose, and dipotassium phosphate. Plates of TSA were prepared using the following methodology.

- 2 g of TSA media powder was dissolved in 50 mL of distilled water
- The solution was autoclaved at 121°C for 40 minutes, then allowed to cool such that it could be safely handled
- TSA was poured slowly into petri dishes to avoid bubbles forming and left to set for approximately 2 h

Media used in doping experiments were prepared using the same procedure, but the dopant was first dissolved into the distilled water at the noted concentration before the addition of the TSA powder.

3.2.2 Bacterial Growth

Bacteria were stored in suspension in distilled water during which time they were metabolically dormant. To grow more, a disposable inoculating loop was dipped into the suspension, then dragged gently across the surface of the TSA plate in order to deposit bacterial cells. The loop was rastered across one third of the plate, then the plate was rotated 120°, and the process was repeated with the streaks more spaced out. This streaking procedure is typically used in microbiology because it tends to yield discrete colonies for sampling. For the purposes of this experiment, this is unnecessary. The procedure was eventually changed between experiments to the use of an L-shaped spreader bar to smear 30 μL of suspension deposited by micropipette across the surface of the plate. These plates were then incubated at 37°C for 24 h for growth. When using the inoculating loop, *P. aeruginosa* and *M. smegmatis* needed to be incubated for 48 h to achieve the same growth on the plate. After growth, bacteria were harvested using a sterile wooden stick and transferred to a 1.5 mL microcentrifuge tube containing distilled water.

For doped samples, additional rinsing steps were added to ensure any signal received from the dopant was from atoms taken up by the cell, not just material adhered

to the surface of the membrane. To rinse, the samples were centrifuged at 3000 rpm for 5 minutes to pelletize the bacteria. The supernatant was then discarded and replaced with fresh distilled water. The sample was then suspended in the fresh water by vortex mixing. This process was repeated three times.

3.2.3 Target Preparation

Bacterial targets were mounted on 13 mm diameter nitrocellulose filter paper. This was done in an effort to bring the procedures used in LIBS more in line with those typically used by diagnosticians. A bacterial suspension was vortexed to create a homogeneous distribution of cells through the solution. A circular metal jig with three 4.7 mm diameter wells drilled through it (shown in Figure 3.7(a)) was placed on top of the filter paper and 30 μL of suspension was deposited in each well via micropipette. The

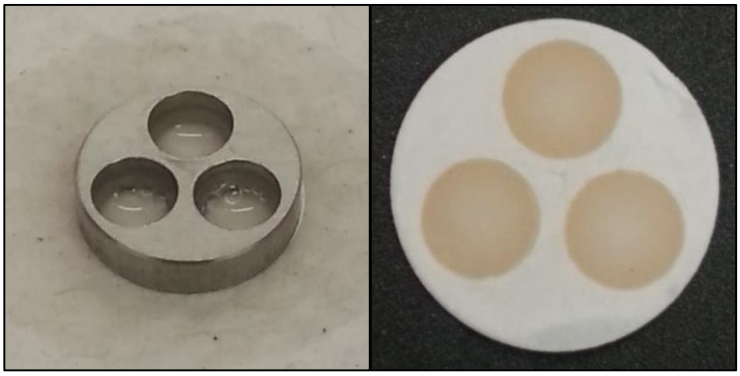

Figure 3.7: (a) Bacterial suspension in the three wells of the metal jig. Water is allowed to pass through the filter to the paper towel beneath. (b) After filtration, three bacterial lawns are left on the filter. These are used for LIBS sampling

suspension was allowed to settle through the filter over approximately 20 minutes, creating three smooth, glasslike bacterial lawns, shown in Figure 3.7(b). The filter was allowed to further dry for one hour and attached to a small steel plate using double-sided tape, and this was placed on the magnetic pedestal inside the argon purge chamber. It was found to be important to allow the filter to fully dry, as a wet filter consistently resulted in lower overall emission intensity. While low intensity could be caused by several effects, wet filter paper gave a characteristic enhanced emission from the hydrogen beta line due to the increased presence of hydrogen in the plasma from the H_2O molecules. The hydrogen beta emission at 482.5 nm is shown in Figure 3.8.

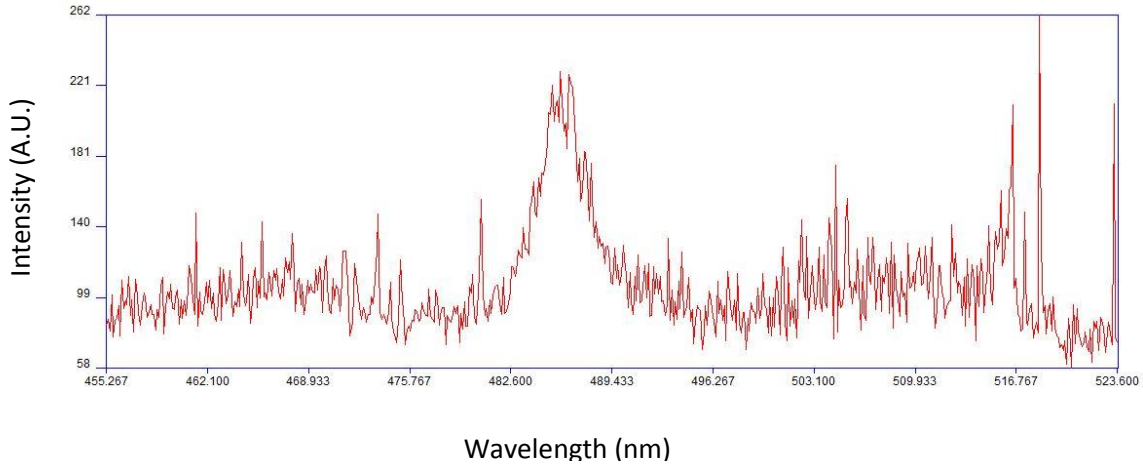

Figure 3.8: Emissions observed from hydrogen beta in a dry sample. Because the line is so affected by Stark broadening, it is not useful for our purpose.

Spectra from bacteria were collected by sampling at three locations on the filter, moving the translation stage 0.635 mm between laser pulses and averaging the spectra collected from the three LIPs through the ESAWIN software. A typical bacterial spectrum is shown in Figure 3.9. Timing settings for data collection were τ_d=2 μs and τ_w=20 μs.

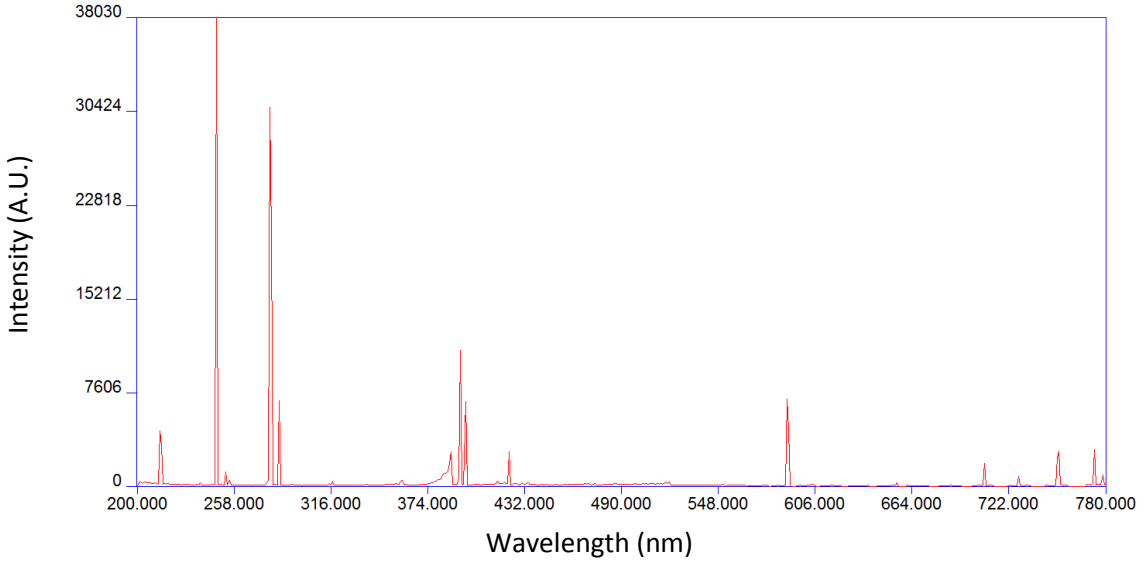

Figure 3.9: A typical LIBS spectrum acquired from an *E. coli* specimen

Amplification was set such that our signal was maximized without saturating the ICCD chip on any emission lines. In bacterial LIBS spectra, 19 lines were regularly observed from carbon, phosphorus, magnesium, calcium, and sodium. Specific lines are noted in the

table below. These lines showed a typical fractional standard deviation of 25-35% across a single filter of bacteria, but this value was dependent on the total number of cells

Table 3.1: Atomic and ionic emission lines observed in LIBS plasmas generated in this work

Element	Ionization State	Wavelength (nm)	Element	Ionization State	Wavelength (nm)
C	I	247.856	Mg	II	280.271
P	I	213.618	Mg	I	277.983
P	I	214.914	Mg	I	285.213
P	I	253.398	Ca	II	317.933
P	I	253.56	Ca	II	393.366
P	I	255.326	Ca	II	396.847
P	I	255.491	Ca	I	422.673
Mg	II	279.079	Na	I	588.995
Mg	II	279.553	Na	I	589.593
Mg	II	279.806			

ablated. To account for this, the intensities were normalized to the total spectral intensity, as with the steel spectra noted above. After this normalization, standard deviations were reduced to 10-20%.

3.2.3.1 Bacterial Lawn

Several samples of *E. coli* prepared using the above method were imaged using the scanning electron microscope (Quanta 200 FEG, FEI) at the Great Lakes Institute for Environmental Research (GLIER). No further preparation was performed with the samples before imaging. As can be seen in the images shown in Figure 3.10, the bacteria formed a

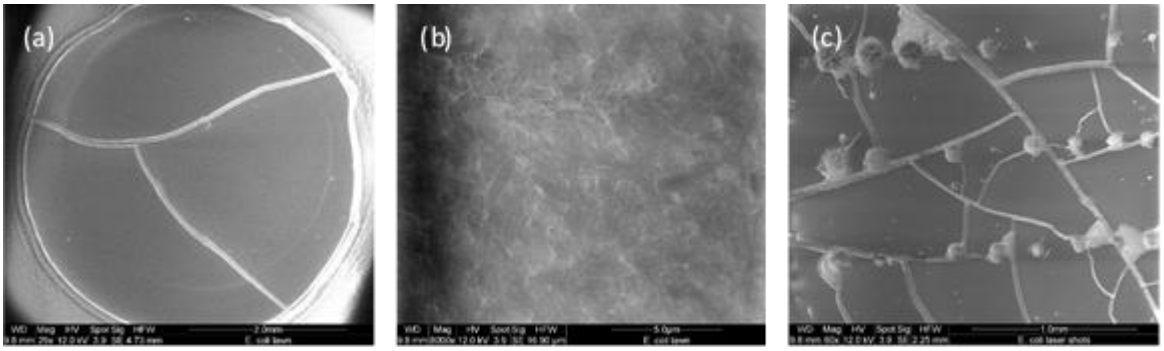

Figure 3.10: SEM images of the bacterial lawn deposited on filter paper. (a) At a low magnification, the lawn appears smooth, but several cracks are observed that sometimes form with drying. (b) At higher magnification, bacteria appear to lie in a uniform coverage across the lawn. (c) Ablation results in non-uniform crater sizes. More cracks in the lawn appear around the craters, including some portions on the lawn that appear to have been blown away

uniform and smooth surface. Images from a lawn taken after ablation in Figure 3.10(c) can be seen to have cracked and shattered around the ablation site. These craters were measured to have a diameter of approximately 150 microns. This shows the difference in laser interaction with the lawn as compared to a bare filter where the ablation crater diameter was consistently measured to be 50 microns.

Investigating the regions around ablation craters, it was seen that the bacteria were melted together, and no debris from the ablation could be seen (Figure 3.11). For this reason, it was assumed that each ablation event could be considered entirely independent, sampling only the bacteria from that location and not fragments deposited from prior ablations. The shape of the craters, however, was not uniform, indicating that

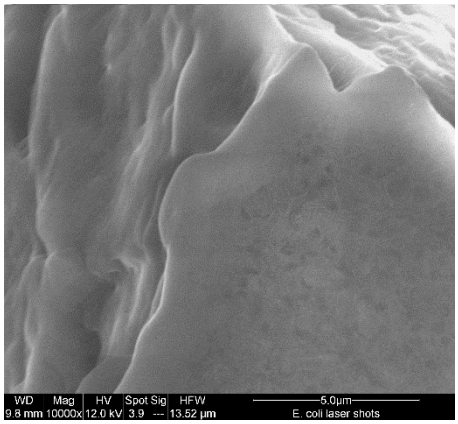

Figure 3.11: At the edges of ablation craters, melting is observed in the bacterial lawn. No debris is observed, and bacteria several microns from the ablation event appear unaffected

the process of energy absorption from the laser by the lawn is not as regular as that of the steel. This serves as a partial explanation of why the variance in the measured bacterial signal is greater than that of the steel.

Further samples were imaged for comparison to the images above after various treatments for the purposes of deactivation of the bacteria or sterilization. These will be discussed later in the thesis when their context is more readily apparent.

References

[1] M. Baudelet *et al.*, Appl. Phys. Lett., **88**, 063901 (2006)

[2] J. Diedrich and S.J. Rehse, J. Appl. Phys., **102**, 014702 (2007)

[3] P. Sivakumar *et al.*, Astrobiol., **15** (2), 144 (2015)

[4] T. Kim *et al.*, J. Phys. Chem. B, **108**, 5477 (2004)

[5] D.W. Merdes *et al.*, Spectrosc., **22** (4), 28 (2007)

[6] M.J. Porter, Astrophys. Space Sci., **273**, 217 (2000)

[7] *Installation Guidelines Échelle Spectra Analyzer ESA 3000*, LLA Instruments GmbH, Berlin, Germany, 2005

[8] *ESAWIN Software Manual Version 3.20*, LLA Instruments GmbH, Berlin, Germany, 2005

Chapter 4: Chemometric Techniques

4.1 Methods for Bacterial Discrimination in LIBS

Since Hybl and Samuel's initial works in bacterial discrimination via LIBS in 2003, many mathematical methods have been explored for differentiating bacterial LIBS spectra. Early methods included the comparison of the ratios of emission lines directly in a two dimensional plot for the discrimination of four species of *Bacillus* and *E. coli* and Baudelet's TEHC wherein the summed emissions of all lines from six elements identified with the bacteria were used as coordinates in a six-dimensional hyperspace.[1, 2] Identification was performed based on proximity to the mean value of a given species. Several more traditional multivariate chemometric techniques for classification were quickly adopted, including the use of principal component analysis (PCA),[3, 4, 5] discriminant function analysis (DFA),[6-10] and partial least squares discriminant analysis (PLS-DA).[5, 9, 11] Several groups have also made use of neural networks for their discrimination, including Manzoor's work, wherein spectra were used to discriminate between bacteria differing only by a single gene mutation.[12, 13]

In this chapter, I will discuss the data model chosen to represent the acquired spectral data and the techniques used for discrimination in this work.

4.2 Data Model

Early LIBS experiments by our group performed chemometric analysis using the intensity of peaks of interest from the spectra normalized to the sum of these intensities.[6] This method used the 13 most intense emission lines resolvable by the apparatus and was named the "lines" model. While this data model provided a fairly robust classification, a new model was created based on the work of Gottfried et al. in explosive detection.[11, 14] This model, named ratio model 1 (RM1), used summed intensities across elements to create five variables, P, C, Mg, Na, and Ca. The number of variables was then increased by making use of complex ratios of these sums for a total of 24 variables. RM2 was constructed using a total of 80 variables, 13 of which were given by the normalized intensity of the lines of interest used in the lines model while the remaining 67 were

formed by simple ratios of line intensities. This model was found to give the most robust classification. The evolution of this data model is discussed in more detail elsewhere.[9]

With the addition of matched parabolic reflectors to the experimental apparatus after its reassembly at the University of Windsor, the apparatus was found to be able to regularly resolve an additional six spectral lines. This lead to the construction of RM3 using 19 normalized peak intensities and their simple ratios. This gives a total of 164 independent variables. The variables used in this model based on the intensities we regularly measure in our plasmas are noted in tables 4.2 and 4.3 at the end of this chapter.

4.3 Classification Algorithms

This work employed two algorithms for classification of bacterial genera: discriminant function analysis (DFA) and partial least-squares discriminant analysis (PLS-DA). Both methods use a pre-compiled library in order to build an "identity" for the groups in the classification. Data is passed to the algorithm in the form of two matrices. The x-block of data is a rectangular matrix containing row vectors that represent our data model.

	C247 (c	P213 (p1)	P214 (p2)	P253.3 (p3	P253.5 (p4	P255.3(p5)	P255.4 (p6	g279 (mgii	g279.5 (mgii	g279.8 (mgii	g280 (mgii	g277(mgi	g285 (mg
102314_ecoli_042	1	0.2859	0.0235289	0.0144224	0.0018586	0.0082139	0.0032144	0.0016665	0.0031805	0.203930718	0.007106702	0.11548109	0.0013954	0.0586557
102314_ecoli_043	1	0.2637	0.0240145	0.0161331	0.0014717	0.0085571	0.003309	0.0014254	0.00498894	0.233906275	0.00908931	0.13530299	0.0017355	0.0522311
102314_ecoli_044	1	0.233	0.0222583	0.0148595	0.0021854	0.0090176	0.0032852	0.0016378	0.00359468	0.207504499	0.006660826	0.12070903	0.0020187	0.0642658
102314_ecoli_045	1	0.2488	0.0239125	0.0147504	0.0018844	0.0093029	0.0035793	0.0014512	0.0051334	0.224569315	0.009459964	0.13480043	0.0021389	0.0509983
102314_ecoli_046	1	0.3051	0.0272667	0.0174771	0.0019862	0.0093434	0.003818	0.0017288	0.00335042	0.209682332	0.006198323	0.1247721	0.0018961	0.0510156
102314_ecoli_047	1	0.3242	0.0274348	0.0161762	0.002193	0.0100582	0.0036566	0.0014333	0.00358572	0.215006331	0.007434794	0.12280577	0.0017726	0.0511319
102314_ecoli_048	1	0.3229	0.0249019	0.0149328	0.0019947	0.0075033	0.0032414	0.0012329	0.00632128	0.279872559	0.011963799	0.1387773	0.001279	0.0319666
102314_ecoli_049	1	0.4049	0.0220988	0.0140322	0.0012902	0.0063425	0.0032426	0.0010961	0.00750137	0.257718305	0.013815309	0.14355933	0.0014672	0.0232976
060414staph_001	2	0.308	0.0424523	0.028774	0.0026525	0.0145992	0.0056275	0.0025591	0.00674365	0.237665932	0.012566365	0.13450382	0.0013156	0.0350551
060414staph_002	2	0.2827	0.0456773	0.0295786	0.0030046	0.0143287	0.0059032	0.0023198	0.00540642	0.217727856	0.010436661	0.12425125	0.0017025	0.0495452
060414staph_003	2	0.2627	0.0456052	0.0302805	0.0028022	0.0134811	0.0052818	0.0029635	0.00538782	0.222831623	0.009761673	0.12815998	0.0018436	0.0515829
060414staph_004	2	0.278	0.0424819	0.0302848	0.0031983	0.0152282	0.0053531	0.0024936	0.00355521	0.191114223	0.006627064	0.11290403	0.0018747	0.0603709
060414staph_005	2	0.2448	0.0419151	0.0279504	0.0038218	0.0152249	0.0051276	0.0027406	0.0030982	0.202776322	0.006034217	0.12391147	0.0022374	0.0595021
060414staph_006	2	0.2665	0.0403921	0.0249962	0.0027382	0.0129727	0.0048338	0.0018856	0.00552252	0.209435737	0.00940718	0.12239048	0.0021754	0.0584715
060414staph_007	2	0.2745	0.0420481	0.0291388	0.0034494	0.0150908	0.0055558	0.002586	0.00362462	0.190365758	0.007528707	0.11185865	0.001585	0.0536818
060414staph_008	2	0.2509	0.0337414	0.0256172	0.0031674	0.012279	0.0052448	0.0021596	0.00320857	0.17738162	0.006797649	0.10829447	0.0018408	0.0639401
060414staph_009	2	0.2658	0.043308	0.0279819	0.0028137	0.0140972	0.0056102	0.0022739	0.00434688	0.185101178	0.008395158	0.10848244	0.0016021	0.0579392

Figure 4.1: Example data from the bacterial library. The first column shows the file name for the spectrum, while the second (marked in red) provides a numerical species label. The rest shows a portion of the x-block (in blue), in this case representing the spectral data

The y-block is a single column vector ordered with the corresponding group identity in the form of a numerical label. Using this data, a model is constructed that is used to determine group identity for an unlabeled spectrum. A screenshot of what this model looks like is shown in Figure 4.1.

To define a quality of classification, an external validation was performed for each algorithm. In an external validation, a portion of the data is removed from the library for the purposes of model construction. A new model is developed, and the x-block of the withheld data is fed into the model. The model's classification is then recorded for the

withheld data. Our external validations withheld data based on the filter from which the data was taken. This is because it should be expected that all data from a single instance of data collection should have similar characteristics. A spectrum acquired from the same bacterial lawn should classify with the rest of its set, so if half of the lawn is in the model, a positive result becomes suspect. External validation guarantees similarities in spectra are reproducible on a day-to-day basis.

Once classification is performed through external validation, truth tables can be constructed for each group. A truth table lists the rate of true positives, correct classifications; false positives, when a non-member is classified in the group; true negatives, when a non-member is excluded from the group; and false negatives, the rate of members being classified outside of the group. This is not a convenient metric, however, as it gives four values per group. Instead, these values are used to calculate a sensitivity and specificity. The sensitivity measures the rate of true positives as a fraction of condition-positive samples. The specificity is the opposite, measuring true negatives as a fraction of condition-negative samples. A weighted average for these values across groups is then calculated. Our goal is to develop a test with a high sensitivity and specificity, meaning that it provides the correct answer reliably with a low number of false positives.

4.3.1 Discriminant Function Analysis (DFA)

Discriminant function analysis can be used to classify between *N* groups, but for the purposes of discussion, we will begin with two groups and extend out from there. Based on the initial library of data, a DFA gives a discriminant score to an unknown row vector *X* that gives its closeness to either group *A* or *B*. The score is often scaled by a constant term such that the score is given by

$$D_{AB} = (\bar{X}_A - \bar{X}_B) \cdot S^{-1} \cdot X^T - \frac{1}{2}(\bar{X}_A - \bar{X}_B) \cdot S^{-1} \cdot (\bar{X}_A + \bar{X}_B) \qquad (1)$$

where $\bar{X}_A$and $\bar{X}_B$are the average vector of independent variables for groups *A* and *B*, X is the unknown to be classified, and S gives the pooled variance-covariance matrix for the groups, defined as

$$S = \frac{(N_A - 1)S_A + (N_B - 1)S_B}{N_A + N_B - 2} \quad (2)$$

and

$$S_{Aij} = covariance(x_{Ai}, x_{Aj}) \quad (3)$$

The second term in the discriminant score simply scales it such that a positive score indicates membership in group *A* and a lower score indicates membership in group *B*.[15]

The discriminant score, loosely speaking, projects unknown data onto a line connecting the midpoint of each known group. The inclusion of the pooled variance-covariance matrix scales the score based on the variance within each group. Other discrimination techniques, such as principal component analysis, will place a datum in a group based simply on which mean is closest. This means that if *A* is well contained but *B* is spread out, a point contained in the spread of *B* may not be correctly classified without considering the pooled variance-covariance matrix.

When expanding out to a system of *N* groups, there exist ${}_NC_2$ discriminant scores. However, only *N-1* scores are needed for classification. This creates an *N-1* dimensional space where an unknown belongs to the group for which the distance between it and the group mean is minimized. As in the two dimensional case, a simple Euclidean distance does not adequately describe this system, so a data point is classified as part of the group for which the Mahalanobis distance, defined as

$$d_A^2 = (X - \bar{X}_A) \cdot S_A^{-1} \cdot (X - \bar{X}_A) \quad (4)$$

for group *A* and similarly for each other group, is minimized.[15] In the statistical analysis software used for this work, the discriminant scores were numbered in decreasing order of relevance to the discrimination. This means that the discriminant score provided by "discriminant function 1" encompasses the largest part of the variance between groups, and each subsequent function's associated score corresponds to a finer degree of detail. Figure 4.2 shows a plot of the first two discriminant functions for a four-group classification conducted as a part of this work.

This method for classification comes with several requirements the data must meet. First is the requirement of not over-determining the system. At minimum, there must be as many data sets in each group for the library as there are independent variables.

An ideal system has as many as four to five times as many samples as variables.[16] The second requirement is that the data be approximately normally distributed. This comes from the fact that the discriminant score function is derived from a Gaussian probability density function for the likelihood of group membership in a particular group given the

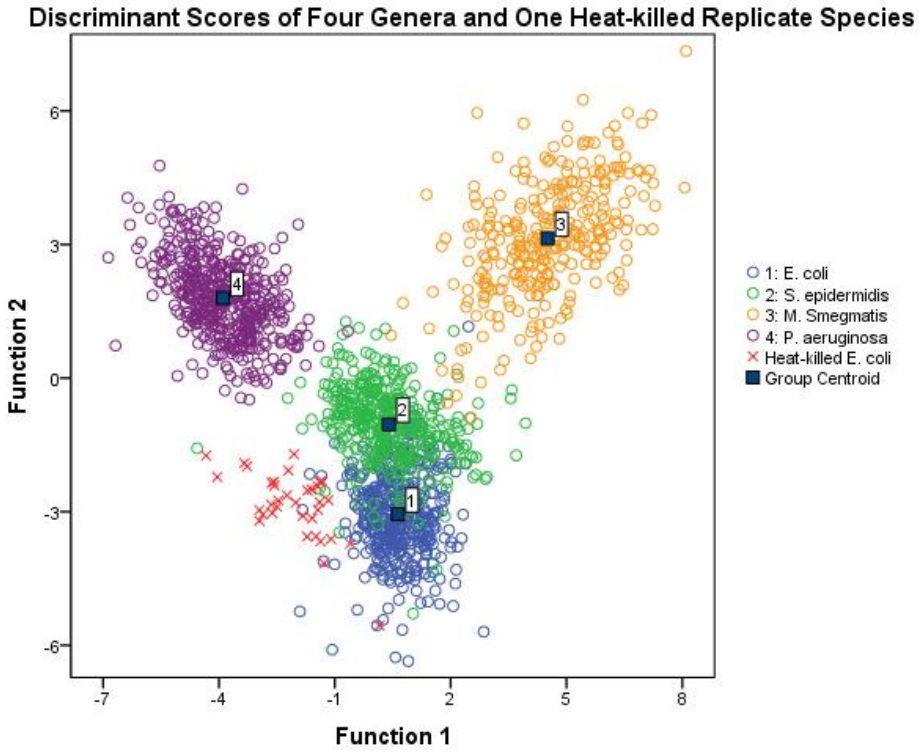

Figure 4.2: DFA plot of four genera of bacteria. Heat-killed *E. coli* were added to the data set for classification without a data label, so a group centroid is not provided

input data.[17] This also leads to the fact that DFA is highly sensitive to outliers. The final requirement of a DFA is that there not be a multicollinearity between variables, that is, no variable can be a simple sum or multiple of another variable.

In my analysis, DFA was performed using SPSS Statistics v.21 (IBM, Inc.).

4.3.2 Partial Least-Squares Discriminant Analysis (PLS-DA)

Partial least-squares is a type of multivariate linear regression technique typically used to construct calibration curves based on spectral data. It is a variable reduction technique that functions much as its original name, projection to latent structures, would imply, by constructing latent variables that maximize the covariance of the x- and y-blocks

of data.[15] This can then be used for discrimination by replacing the continuous data in the y-block with two values, usually +1 and -1 or 1 and 0, to represent a "yes" and a "no" class. Once the regression is performed, a threshold value is determined by Bayesian statistics to define the border between the two groups. An unknown data point is then given a "predictor value" based on the regression. If this predictor value falls above the threshold, the test result is positive; the datum is classified as a member of the group. Unlike DFA, this procedure is not extended to multiple classes but is instead performed once per class. The test is run as a yes or no question of group *A* membership, then of group *B*, then *C*, and so on. As a result, PLS-DA provides a potential null result that isn't possible with a DFA.

While there are several methods for performing PLS-DA, all still hold many of the same requirements as DFA. Primarily, it is important to avoid overfitting the data by using fewer independent variables than data files in each class in the library used to construct the discrimination model. Overfitting primarily leads to an increased rate of false positive results.[18]

PLS was performed using the PLS_toolbox v6.7.1 running under Matlab v7.6 (Eigenvector Research, Inc.).

4.4 Initial Discrimination Results

In previous experiments by this group, LIBS classification data were collected using bacteria mounted on a background-free bacto agar medium. In my study it was important to ensure that the addition of a strong carbon background signal from the nitrocellulose filter would not strongly interfere with the discrimination. For my primary results, a library of spectral data from the four bacterial species, *E. coli*, *S. epidermidis*, *M. smegmatis*, and *P. aeruginosa*, was collected over the course of three months. For each species, multiple plates of bacteria were grown to maximize the variation between samples. Both of these measures ensure that any similarities observed in the data are characteristic of the bacteria by ensuring day-to-day variation. Approximately 350 spectra, each the averaged spectrum of three plasmas on the filter, were collected per species for a total library of 1514 files.

This library was analyzed using both DFA and PLS-DA to determine if one method provided significantly better classification than the other as well as to determine the quality of the library for discrimination. In both cases, the analysis was an external validation performed by withholding all files taken from a single filter paper in a single instance of data collection. Through this analysis, it was determined that through DFA, a sensitivity of 98±2% and a specificity of 99±1% could be achieved. A similar result, sensitivity of 97±3% and specificity of 99±2%, was achieved through PLS-DA. The full truth tables for each classification are provided below.

Table 4.1: Truth tables for discrimination of four genera of bacteria mounted on nitrocellulose filters using (a) DFA and (b) PLS-DA

(a)

Escherichia	TRUE	FALSE	*Staphylococcus*	TRUE	FALSE
Positive	98.28%	0.77%	Positive	97.75%	1.44%
Negative	99.23%	1.72%	Negative	98.56%	2.25%
Mycobacterium	TRUE	FALSE	***Pseudomonas***	TRUE	FALSE
Positive	95.36%	0.33%	Positive	99.57%	0.22%
Negative	99.67%	4.64%	Negative	99.78%	0.43%

Sensitivity: 98 ± 2% Specificity: 99 ± 1%

(b)

Escherichia	TRUE	FALSE	*Staphylococcus*	TRUE	FALSE
Positive	96.55%	1.12%	Positive	96.75%	1.53%
Negative	98.88%	3.45%	Negative	98.47%	3.25%
Mycobacterium	TRUE	FALSE	***Pseudomonas***	TRUE	FALSE
Positive	97.02%	0.41%	Positive	98.92%	0.33%
Negative	99.59%	2.98%	Negative	99.67%	1.08%

Sensitivity: 97 ± 3% Specificity: 99 ± 2%

These results show that the use of a nitrocellulose filter paper as a mounting medium for LIBS on bacteria not only moves this technique closer to one that might be used in a clinical setting, but the classification of this data is, within error, perfectly accurate, although admittedly this is only true for the four organisms tested in this study.This result can be compared to this group's previous work with a background-free mounting procedure, wherein a sensitivity and specificity of 91±16% and 98±9% was achieved using a DFA under RM2.[9]

This result also shows no measurable difference in the performance of DFA as compared to PLS-DA. While the two procedures performed identically within error, DFA performed nominally better. For this reason, classification for the remainder of this work was performed primarily using DFA.

Table 4.2: Emission lines used for discrimination and the variable names associate with each. The following figure will use these designations to describe the ratios used in RM3

Emission Line	Variable Designation
C 247.856	c
P 213.618	p1
P 214.914	p2
P 253.398	p3
P 253.56	p4
P 255.326	p5
P 255.491	p6
Mg 279.079	mgii1
Mg 279.553	mgii2
Mg 279.806	mgii3
Mg 280.271	mgii4
Mg 277.983	mgi1
Mg 285.213	mgi2
Ca 317.933	caii1
Ca 393.366	caii2
Ca 396.847	caii3
Ca 422.673	cai1
Na 588.995	na1
Na 589.593	na2

Table 4.3: Ratios used for discrimination in RM3

p1/c	p2/na2	p4/na1	p6/cai1	mgii4/caii2	caii3/na2
p1/mgii1	p3/c	p4/na2	p6/na1	mgii4/caii3	caii4/c
p1/mgii2	p3/mgii1	p5/c	p6/na2	mgii4/caii4	caii4/na1
p1/mgii3	p3/mgii2	p5/mgii1	mgii1/c	mgii4/cai1	caii4/na2
p1/mgii4	p3/mgii3	p5/mgii2	mgii1/caii2	mgii4/na1	cai1/c
p1/mgi1	p3/mgii4	p5/mgii3	mgii1/caii3	mgii4/na2	cai1/na1
p1/mgi	p3/mgi1	p5/mgii4	mgii1/caii4	mgi1/c	cai1/na2
p1/caii2	p3/mgi	p5/mgi1	mgii1/cai1	mgi1/caii2	c/na1
p1/caii3	p3/caii2	p5/mgi	mgii1/na1	mgi1/caii3	c/na2
p1/caii4	p3/caii3	p5/caii2	mgii1/na2	mgi1/caii4	mgi1/mgii1
p1/cai1	p3/caii4	p5/caii3	mgii2/c	mgi1/cai1	mgi1/mgii2
p1/na1	p3/cai1	p5/caii4	mgii2/caii2	mgi1/na1	mgi1/mgii3
p1/na2	p3/na1	p5/cai1	mgii2/caii3	mgi1/na2	mgi1/mgii4
p2/c	p3/na2	p5/na1	mgii2/caii4	mgi/c	mgi/mgii1
p1/mgii1	p4/c	p5/na2	mgii2/cai1	mgi/caii2	mgi/mgii2
p2/mgii2	p4/mgii1	p6/c	mgii2/na1	mgi/caii3	mgi/mgii3
p2/mgii3	p4/mgii2	p6/mgii1	mgii2/na2	mgi/caii4	mgi/mgii4
p1/mgii4	p4/mgii3	p6/mgii2	mgii3/c	mgi/cai1	cai1/caii2
p2/mgi1	p4/mgii4	p6/mgii3	mgii3/caii2	mgi/na1	cai1/caii3
p2/mgi	p4/mgi1	p6/mgii4	mgii3/caii3	mgi/na2	cai1/caii4
p2/caii2	p4/mgi	p6/mgi1	mgii3/caii4	caii2/c	
p2/caii3	p4/caii2	p6/mgi	mgii3/cai1	caii2/na1	
p2/caii4	p4/caii3	p6/caii2	mgii3/na1	caii2/na2	
p2/cai1	p4/caii4	p6/caii3	mgii3/na2	caii3/c	
p2/na1	p4/cai1	p6/caii4	mgii4/c	caii3/na1	

References

[1] T. Kim *et al.*, J. Phys. Chem. B, **108**, 5477 (2004)

[2] M. Baudelet *et al.*, Appl. Phys. Lett., **89**, 163903 (2006)

[3] J.D. Hybl, G.A. Lithgow, and S.G. Buckley, Appl. Spectrosc., **57** (10), 1207 (2003)

[4] A.C. Samuels *et al.*, Appl. Opt., **42** (30), 6205 (2003)

[5] D.E. Lewis *et al.*, Anal. Bioanal. Chem., **401**, 2225 (2011)

[6] J. Diedrich and S.J. Rehse, Appl. Phys. Lett., **90**, 163901 (2007)

[7] C. Barnett *et al*., Anal. Bioanal. Chem., **400**, 3323 (2011)

[8] D.W. Merdes *et al.*, Spectrosc., **22** (4), 28 (2007)

[9] R.A. Putnam *et al.*, Spetrochim. Acta, Part B, **87**, 161 (2013)

[10] Q. Mohaidat, S. Palchaudhuri, S.J. Rehse, Appl. Spectrosc., **65** (4), 386 (2011)

[11] J.L. Gottfried *et al.*, Appl. Spectrosc., **62** (4), 353 (2008)

[12] D. Marcos-Martinez *et al.*, Talanta **84**, 730 (2011)

[13] S. Manzoor *et al.*, Talanta, **121**, 65 (2014)

[14] J.L. Gottfried *et al.*, Appl. Spectrochim. Acta, Part B, **62**, 1405 (2007)

[15] R.G. Brereton, *Applied Chemometrics for Scientists*, 1st Ed. (West Sussex, England, 2007)

[16] J. Poulsen and A. French, *Discriminant Function Analysis (DA)*, <http://userwww.sfsu.edu/efc/classes/biol710/discrim/discrim.pdf> (2004)

[17] *Applied Multivariate Statistical Analysis Course Materials*, PennState Eberly College of Science, <https://onlinecourses.science.psu.edu/stat505/node/89> (2016)

[18] M. Grootveld, *Metabolic Profiling: Disease and Xenobiotics*, 1st Ed. (Cambridge, England, 2014), pp. 18-20

Chapter 5: Concentration Study[i]

5.1 Introduction

While it has been shown that bacteria can be identified based on their so-called spectral fingerprint, it is important to note that these experiments typically use large quantities of pure bacteria for sampling. In contrast, clinical samples retrieved via nasal swab for methicillin-resistant *S. aureus* (MRSA) typically contain between 0 and 200 colony forming units (CFU).[1] It is therefore important to quantify a limit of detection for bacterial cells in this system. For this purpose, samples of bacteria were serially diluted, and a calibration curve was constructed based on the response of the LIBS apparatus to various titer. Titer is a standard method for measuring dilution in microbiological applications, where concentration is expressed as a ratio of dilutant to total suspension volume.

In LIBS, a calibration curve typically has a linear dynamic range, wherein the signal from a line of interest has a simple linear relationship to the amount of material ablated, typically measured as a mass or a concentration. In a high concentration regime, this response becomes saturated due to self-absorption. Self-absorption is an effect of the temperature difference between the core of the plasma and its outer edges. Since the outer shell of the plasma is largely populated by relatively cool atoms, photons emitted from the core are typically reabsorbed before reaching the light collection apparatus, resulting in a decrease in the measured signal and causing a saturation plateau in the measured calibration curve.[2]

5.2 Methods

For the purposes of the calibration curve, only *E. coli* was explored, as other bacteria are of similar volumes to within the same order of magnitude.[4-7] One plate of *E. coli* was cultured and placed in suspension as per the procedure discussed in chapter three. This suspension was defined to be a concentration of 1 (A.U.). Serial dilutions in

[i] These experiments were the result of collaboration with D.J. Gillies and were published earlier this year.[3]

distilled water were performed to generate suspensions of concentrations of $c = \{1, 1:10, 3:40, 2:30, 1:20, 1:30, 1:40, 1:80, \ 1:100, 1:1000\}$. Filters were prepared in the usual manner, with one well being filled with each concentration of suspension. From each of these lawns, 17 averaged spectra were acquired at a constant amplification. A plot was generated by graphing the total spectral intensity, defined as the sum of the area-under-the-curve intensities of the emission lines used in bacterial classification, against the relative concentration. These numbers were then scaled to true concentrations in CFU/mL via optical densitometry performed on dilutions of the initial suspension.[8] Through a geometric argument and the assumption of uniform deposition through the well, this number could then be converted to a number of CFU ablated per shot. This assumption is supported at the full concentration by the images acquired via scanning electron microscopy as shown in figure 5.1. These images were also used to determine ablation crater diameter which was used to calculate the number of CFU ablated per shot. At a concentration of 1 A.U., approximately 10^6 CFU were ablated per laser pulse.

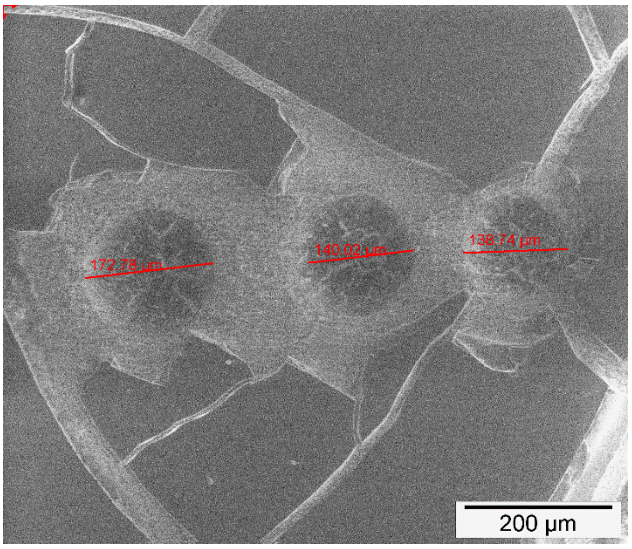

Figure 5.1: SEM images acquired from an *E. coli* lawn that had been ablated. Average crater diameter was found to be approximately 150 microns

Once the plot of measured LIBS intensity versus bacterial concentration was generated, a region of linear dynamic range was identified, and a linear fit was performed. From this fit, a slope and y-intercept error were acquired. The limit of detection was defined as the number of colony forming units required for a 99.7 % confidence that the

measured signal was due to bacteria, not random noise. Mathematically, this limit of detection is typically defined as

$$LOD = \frac{3\sigma}{m} \quad (1)$$

where σ is the error on the y-intercept of the fit and *m* is the slope.[3]

It is important to note that this number is a calculation of the minimum number of cells that provide enough signal to differentiate bacteria from the filter paper background. This does not mean that the species will remain differentiable at this concentration. For this, experiments must be performed to measure a limit of identification which is expected to be a higher concentration. In order to observe the trend shown in a calibration curve, a constant amplification must be used when acquiring data. This results in smaller emission lines used for discrimination fading into noise. For limits of identification, amplification should be maximized at each concentration while avoiding saturation of the detector.

5.3 Results

The calibration curve we obtained is shown in Figure 5.2. The linear dynamic range of our system began at a concentration of 0.1 A.U. and ran through 0.0125 A.U., after which no signal was discernable from that of a blank filter. Since the filter always provided a strong carbon background at all concentrations, our measured signal never decayed to a zero reading for a blank sample (the absence of cells), instead leaving only the 247.856 nm carbon emission line. A linear fit over this range possessed an adjusted r^2 value of 0.979, indicating a strong fit to the expected trend. However, when the errors on the measurements were given direct weighting in the fit, the r^2 dropped to 0.728. What this shows is that while the trend is observed in the average data, there is a wide scatter in these measurements. This more realistic fit gives a limit of detection of 48000±12000 CFU per ablation event. This value is not clinically useful, and efforts must be made to bring this more in line with the amount of bacteria typically obtained from a clinical sample by a diagnostician.

Looking at individual spectra directly, it is clear that at low concentrations, bacteria tend to clump together, with certain spectra showing relatively strong emissions while

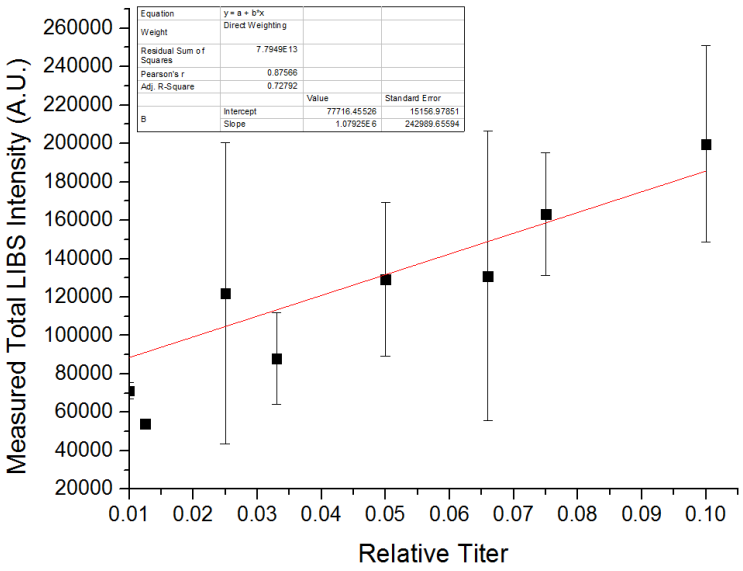

Figure 5.2: Linear fit to the calibration curve data. In this fit, the errors are given direct weight

others were comparable to that of a blank filter. This is shown in figure 5.3 where two spectra from the same bacterial deposition are shown overlapped. The bacteria are initially vortexed in suspension before deposition on the filter paper to minimize clumping, but this does not seem to sufficiently separate the cells. It is also possible that some clumping occurs while the suspension is left to pass through the filter paper. For this reason, a method for deposition may be required that either causes the lawn to form

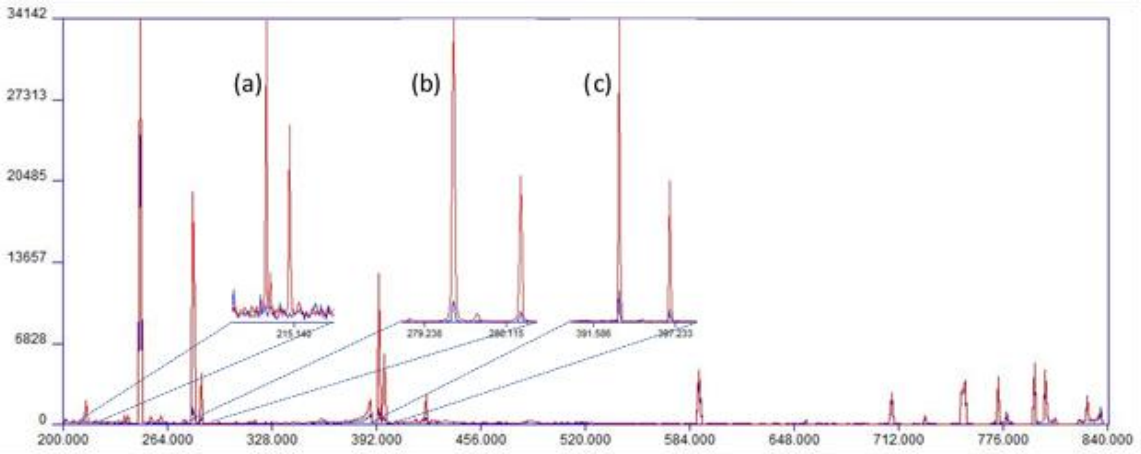

Figure 5.3: Two overlapped spectra in red and blue taken from the same well during data acquisition. The suspension was at a titer of 1:30. Inset are zoomed-in sections showing the strongest emissions from (a) phosphorus, (b) magnesium, and (c) calcium

more quickly, which may help prevent clumping by way of not allowing the bacteria the time required to do so, or one that prevents clumping entirely. The latter may be

accomplished with the addition of the enzyme trypsin to the bacterial suspension. Trypsin is used to dissociate cell colonies and prevent cell adherence to glassware.[9] A method for quickly settling the bacterial suspension onto the filter will be discussed in the next chapter.

No investigations were performed into a limit of identification at this stage. This was for two reasons. Firstly, as the ratio model involves the use of emission intensities in the denominator of ratios, the fact that many lines are no longer resolvable at low concentrations would result in divergence in the data model. This makes discrimination impossible. Secondly, and more practically, since it is expected that the limit of identification will be greater than the limit of detection, a LOD of approximately 50000 CFU would imply that the LOI is not a useful quantity at this stage. Until a more reasonable LOD is achieved, determination of a LOI will not have any value.

References

[1] P. Warnke *et al.*, PLoS ONE, **9** (10), e111627 (2014)

[2] D.A. Cremers and L.J. Radziemski, *Handbook of Laser-Induced Breakdown Spectroscopy*, 1st Ed. (West Sussex, England, 2006)

[3] D.J. Malenfant, D.J. Gillies, and S.J. Rehse, Appl. Spectrosc., **70** (3), 485 (2016)

[4] *Veterinary Biology: Information About Important Bacteria*, Sveriges Iantburksuniversitet <http://www.vetbact.org/vetbact/?artid=205> (2015)

[5] *Veterinary Biology: Information About Important Bacteria*, Sveriges Iantburksuniversitet <http://www.vetbact.org/vetbact/?artid=68> (2016)

[6] *Veterinary Biology: Information About Important Bacteria*, Sveriges Iantburksuniversitet <http://www.vetbact.org/vetbact/index.php?artid=65&vbsearchstring=pseudomonas%20aeruginosa> (2015)

[7] J.A. Gonzalez-y-Merchand *et al.*, J. Microbiol., **50**, 419 (2012)

[8] I. Sondi and B. Salopek-Sondi, J. Colloid Interface Sci., **275**, 177 (2004)

[9] *Trypsin-EDTA (0.25%)*, STEMCELL Technologies Inc, <https://www.stemcell.com/trypsin-edta-0-25.html> (2016)

Chapter 6: Centrifuge Filtration

6.1 Introduction

In the previous chapter, it was theorized that one potential reason for the high standard deviation observed in the intensity measurements for cellular suspensions at low concentrations may have been a result of clumping of cells as the suspension was left in the wells of our steel jig as it settled through the filter paper. This argument is supported by the spectra acquired during the initial calibration curve study.

Since it is believed that clumping was occurring in suspension as bacteria were filtered, I designed an insert to be placed inside a test tube in a centrifuge. This insert would hold a piece of filter paper at its base with suspension to be added above this. Through centrifugation, this suspension could be forced to settle far more quickly. Clumping could then be prevented by creating the lawn before it could occur. This chapter will discuss the design choices made for this insert and the first preliminary results on its efficacy.

6.2 Design

Centrifuge test tube inserts for filtration are currently available on the market, and this design borrows several features from the Sigma-Aldrich Ultrafree-CL microcentrifuge filters (M9160 SIGMA). This product and others like it are meant to be placed in centrifuge tubes and filled with a solution. The tube is then centrifuged, dragging the solution through the filter at the insert's base. These products do not meet our needs, as they are meant as a solution for experiments where it is the filtrate that is of interest. As a result, the insert is sealed, usually through an ultrasonic weld, around the filter paper. In these LIBS experiments, it is the filter that is of interest, and so a design that prevents access to the filter is not useful.

My insert was designed using the SolidWorks 2010 CAD software (Dassault Systémes Solidworks Corporation) and a prototype was generated by Hyphen Services via 3-D printing . This took the same shape as the commercial inserts, but the base could be threaded into the main body of the insert to allow access to the filter. The base of the insert acts as a pedestal on which the filter is placed, and screwing it into the main body

creates a seal around the edge of the filter through applied pressure. A cross-section of this device is shown below. To ensure the fluid in the suspension can freely flow through the filter, the filter is supported by a solid ring around the outer circumference and several small columns placed in three concentric rings in order to prevent the filter from resting

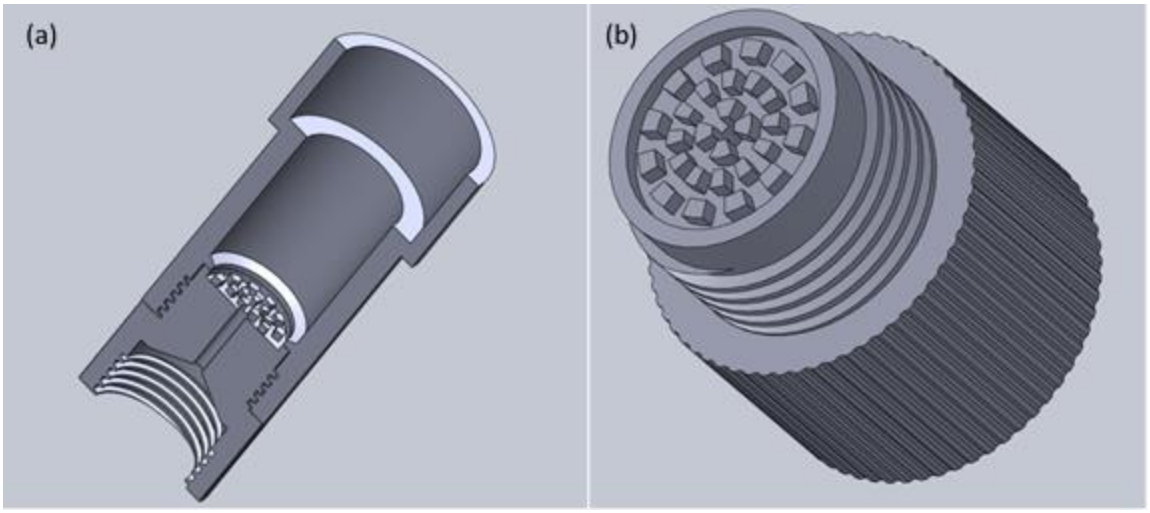

Figure 6.1: (a) Full centrifuge insert design in cross section. Filter paper is placed on the male end (b) of the device, and a seal is produced by the pressure generated by the threads. Pedestals under the filter paper prevent it from resting directly on a flat surface, allowing water to freely pass through the filter

directly on the base. A hole in the middle of the base allows the fluid to then drain out of the insert and into the centrifuge tube in which the insert sits. The base of the tube also has female threads in the bottom. This is for the purpose of tiered filtration for the separation of cells of different sizes that may be mixed in suspension. Since this thesis only addresses pure cultures and the bacteria used are all of similar size, no experiments investigating the efficacy of this feature were performed.

6.3 Filtration

Standard Millipore 0.22 μm pore size nitrocellulose filter paper was used for these experiments. 1.5 mL of *E. coli* suspension was vortexed to achieve nominally uniform suspension, then centrifuged through the insert for 3 minutes at 5000 rpm (2500 gs of force). Leakage through the pressure seal was investigated using optical densitometry on the initial suspension and the filtrate after centrifugation. With ideal functionality, all cells will be caught by the filter, and none will be observed in the filtrate. A calibration curve

for optical density was constructed using a quadratic fit to account for data outside the regime of Beer's Law. This fit over eight concentrations gave an r^2 value of 0.999. Using this fit to calculate concentrations, it was determined that 11% of the cells in the initial suspension somehow bypassed the filter and were found in the filtrate. With an initial suspension concentration of 8×10^8 CFU/mL, this still resulted in a lawn on the filter that yielded 2.5×10^6 CFU per ablation event. This was approximately the bacterial lawn density observed and used in prior experiments. This experiment was repeated at titers of 1:6 and 1:9 to ensure that the fractional loss measured was not a function of initial titer. These experiments yielded a loss of 7.3 and 5.3% respectively.

While this result is preferable to an increase in loss, the fact that loss showed some dependence on concentration means that it is not possible to give precise numbers on deposition at this time. The design of the insert should be updated and another prototype developed to create a stronger seal around the filter. It is, alternatively, possible that the seal is sufficient, and bacteria are instead escaping through the filter directly. Based on the porous nature of the filter observed under SEM, this seems unlikely enough to discount the possibility.

6.4 Signal Regularity

With losses, enough bacteria were deposited on the filter to perform LIBS. However, since the centrifuge held the tube at an angle off from the vertical, it was uncertain if the deposition across the surface of the filter could be assumed to be uniform. As the suspension was pulled through the filter, the fluid level in the centrifuge tube insert dropped. This left the suspension passing only through the bottom segment of the filter. This had the potential result of heavier deposition at one side of the filter paper. For this reason, single shot LIBS data was collected from across an entire filter with sampling locations spaced in a 0.6825 mm (approximately 1/40") square grid. This experiment served as a check that not only was the total spectral intensity uniform spatially on the filter indicating that deposition was regular, but it would also allow for comparison to previous data in terms of the standard deviation of the intensity of the spectral lines

observed. Again, *E. coli* was used as a representative organism as no major variation between genera was expected.

As can be seen in the false-colour map shown in Figure 5.2 no strong patterns emerged in the intensity of the LIBS signal across the filter. There is some increase in intensity from one side of the filter to the other; however, this variation is within the normal variation observed in bacterial plasma intensities. When comparing the fractional standard deviation of the spectral lines to previous data, it was seen that the signal was similarly reproducible. Deviation on atomic lines in the bacterial spectra was normally seen to be 20% for small lines and 5-10% for the more intense lines. When using the centrifuge filter, these values were seen to be 35 and 25% before any averaging. In general, bacterial data was taken as the average of the emissions from three ablation events. Since standard deviation is inversely proportional to $\sqrt{N}$, where N is the number

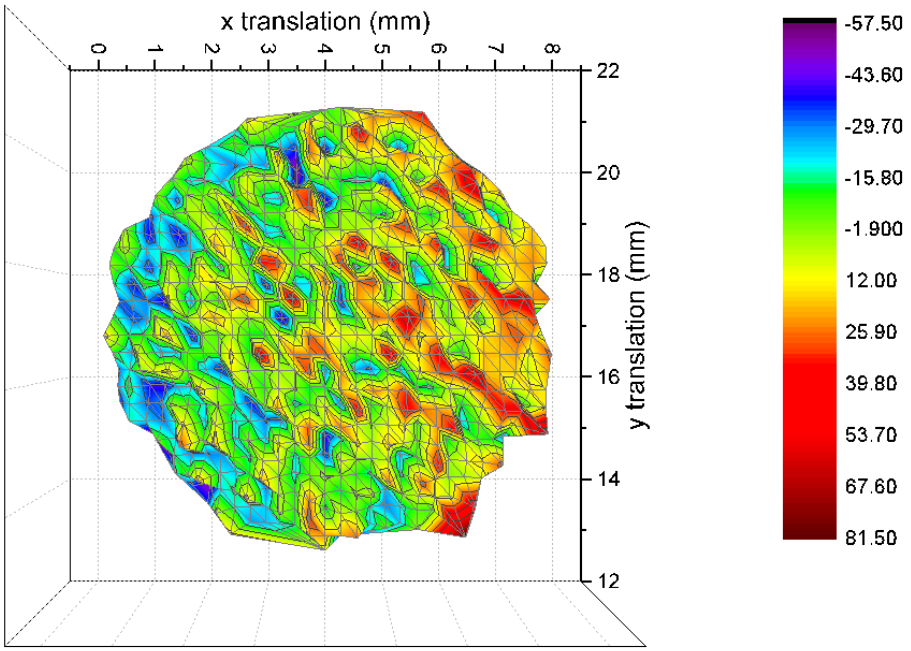

Figure 6.2: Colour map indicating percent difference of the total measured LIBS intensity from the average as a function of position on a nitrocellulose filter. Some increase is observed with motion in the positive x-direction, but this increase spans from approximately -20 to 20% difference from the mean which is within typical variation

of measurements, this averaging can be expected to reduce these standard deviations to approximately 20 and 15%. This indicates that, losses notwithstanding, this mounting method provides a viable method for sample preparation that still makes use of only

techniques that are familiar to clinicians or those used to working in a microbiological laboratory. Since signal appears to be similarly regular when compared to the previous mounting procedure, the centrifuge insert was used to repeat the previous concentration studies.

6.4.1 Calibration Curve

This concentration study measured the total spectral intensity of the LIBS signal across the same concentration range discussed in the previous chapter. Due to the space available on the filter when not using the wells, 35 averaged spectra were acquired at each concentration. The plot of this data is shown in Figure 6.3. It is immediately apparent that this data shows far less variance in low concentrations. When a fit is performed to

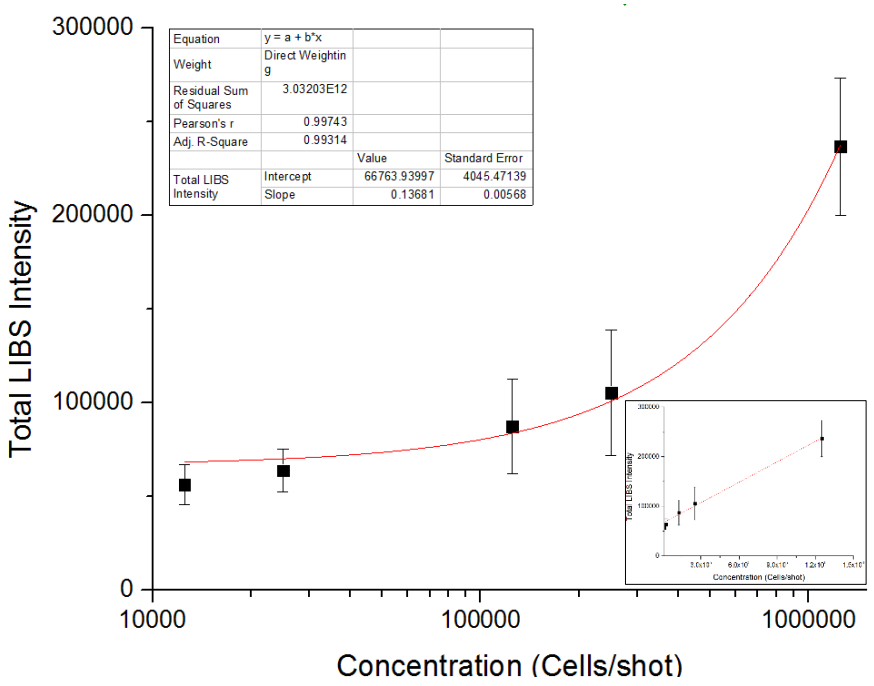

Figure 6.3: Calibration curve for data acquired using specimens prepared with the centrifuge insert. The plot is displayed on a log-lin scale. The inset plot shows the same data on a lin-lin scale

this data, an r^2 value of 0.975 is received. However, on calculating a limit of detection, no improvement over the previous method was observed. Without accounting for error, the LOD was determined to be 60 000 ± 5 000 CFU per ablation event. When error is given a direct weighting on the fit, the goodness of fit improved to an r^2 of 0.993, but the LOD was then calculated as 90 000 ± 9 000 CFU per ablation event. While this is not an encouraging

result from the standpoint of developing a clinical technique, this shows that a number of this magnitude may be a limitation of a filter-based mounting procedure. In previous systems, this may have been overcome with amplification, but the persistent carbon signal of the filter limits the gain that can be used without doing potentially permanent damage to the spectrometer's ICCD chip.

Chapter 7: Elemental and Chemical Doping

7.1 Motivation

The importance of inorganic elements found in the membrane to the classification of bacterial specimens has been demonstrated on many occasions.[1, 2] This has raised the question, however, of bacteria grown in extreme environments. Without sufficient nutrients present, bacteria will not grow. When a surplus of needed nutrients is available, will a visible impact be made on the spectra of the bacteria? This effect has already been observed for some compounds in the processes of biosorption and bioaccumulation. Bioaccumulation is the metabolically active process by which metals are incorporated into the biomass of the cell. Biosorption is the passive compliment to this procedure wherein the metals are instead held at the surface of the cell.[3]

With the uptake of additional metals from the environment, we must be concerned with the alteration of the spectra in a way that will impair our ability to properly discriminate between species. In this chapter, I will discuss experiments performed to ensure that the variation of minerals found within the human body due to diet will not adversely impact bacterial identification for samples taken from a biological system. It is not anticipated that the regular biological concentrations of these atomic species *in vivo* (typically on the order of a few parts per million) will be sufficient to alter spectra in any noticeable way.[4, 5]

Additional experiments were performed using glucose as a dopant in growth medium in order to simulate the ranges of concentration in a healthy patient or one with type 1, or children's type 1 diabetes. Since the transport of many metabolically important metals through the cell membrane is an active process for the cell, providing an excess of glucose may result in changes to the bacterial spectrum due to increased uptake. These results in combination will provide an argument for the viability of LIBS-based identification of bacteria harvested from a biological system such as the human body through a swab or a fluid sample such as urine or cerebrospinal fluid.

Recently, however, the processes of biosorption and bioaccumulation have been demonstrated to be useful for the remediation of heavy metal contamination in the

environment.[6, 7] This provides an opportunity to use LIBS on bacteria as a proxy measurement for environmental metal contamination. For this reason, *E. coli* were also grown in an environment with concentrations of metals on the order of hundreds of parts per million to simulate hard water or an environmental contamination.

These experiments were performed using two metal species: magnesium, chosen because it is used in our discrimination and could be expected to seriously hamper accurate classification, and zinc, not typically observed in our spectra, chosen as a representative contaminant. Both are found within biological systems as well as being common water contaminants for environmental concerns.[8, 9, 10] The intensity of the emissions from these species was monitored as a function of the concentration of the metal ion solution used in the preparation of the agar media on which the bacteria were grown.

7.2 Bacterial Doping at Biological Concentrations

7.2.1 Metal Species

The usual ranges of concentrations for zinc and magnesium concentrations in blood are 0.6 to 1.3 ppm and 1.5 to 2.3 ppm respectively in human blood.[5] Initial experiments were conducted with zinc, as zinc emission is not typically observed in our bacterial spectra. Plates were prepared using zinc solutions ranging from 0.1 to 0.4 ppm and bacterial samples were cultured overnight. Samples at each concentration were then prepared for ablation using the usual methodology. Each of these steps is described in detail in chapter three. For each concentration, 10 spectra were acquired (30 ablation

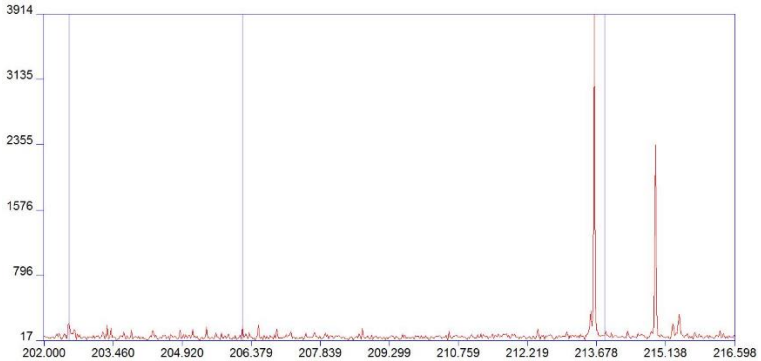

Figure 7.1: Spectrum from *E. coli* doped with zinc at physiological concentrations. Vertical blue lines indicate the expected locations of zinc emissions in the spectrum. No emission is observed

events). These spectra were averaged for noise reduction, but zinc lines remained indistinguishable from the background as seen in Figure 7.1.

Magnesium doping was not performed at biological concentrations. In the same concentration regime, the addition of zinc to the nutrient medium did not provide enough change to cellular composition to create signal distinguishable from noise. Magnesium gives several of the strongest lines present in the bacterial spectrum with a typical variation in intensity of 10%. The addition of such a small quantity of magnesium can be safely assumed to make no difference to the spectral fingerprint of the bacteria and thus have no impact on the discrimination of species.

7.2.2 Glucose

Ion transport across cellular membranes is often an active process requiring an investment of energy by the cell.[11, 12, 13] Glucose concentration in the blood varies over a wide range among humans, from 1.35 g/L in a healthy human to 1.80 g/L in one with children's type 1 diabetes.[14] Bacteria grown in an environment with an excess of glucose may be at a metabolic advantage, able to take up metal atoms more readily. This could, in turn, result in an observable shift in bacterial spectra. For this reason, *E. coli* was grown in environments with excess glucose concentrations shown in the table below. Again, spectra were acquired from each concentration, and a classification was performed.

Table 7.1: Glucose concentrations used for the studies discussed in this chapter

Representative Condition	Sample Concentration (g/L)
Healthy Individual	1.35
Type 1 Diabetes	1.62
Children's Type 1 Diabetes	1.80

Discrimination was performed using DFA and a library of 850 spectra. These data classified correctly as *E. coli* for 82% of the files. This is in keeping with a library sensitivity of 83%. Since the sensitivity gives the idealized rate of true positive classifications for unknown data, this result suggests that any alterations to the emission spectra caused by the addition of glucose to the growth media are not relevant to our discrimination. The discriminant score plot for the classification of *E. coli* grown in conditions representative of children's type 1 diabetes is shown in Figure 7.2.

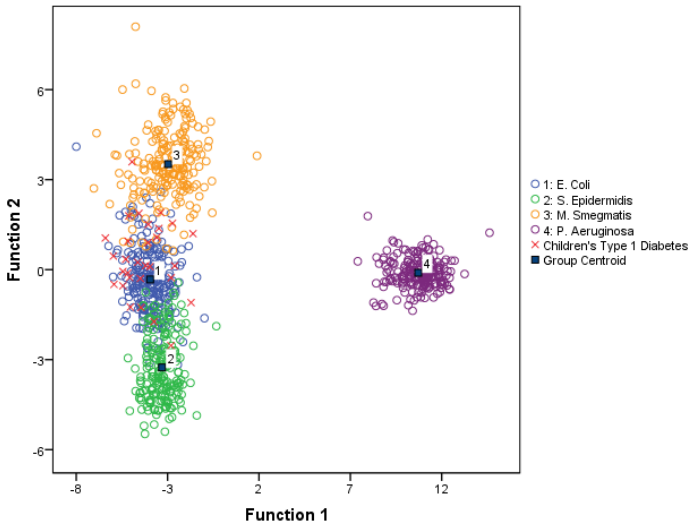

Figure 7.2: DFA Classification of *E. coli* grown in an environment with a glucose concentration representative of children's type 1 diabetes

7.3 Elemental Doping at Environmental Concentrations

7.3.1 Environmental Zinc

While zinc is required for biological function, high levels of zinc can be toxic to both bacteria and humans. Bacteria, through biosorption and bioaccumulation, are also the primary method of self-purification for fresh water.[9] These facts, when coupled, provide both a problem as well as a probe. These experiments are meant to probe the possible utility of LIBS on bacteria as a measure of water quality. *E. coli* was grown on the typical TSA medium prepared in zinc sulfate solution of concentrations 0, 100, 200, and 300 ppm. These represent concentrations far greater than those typically found in nature.[10] These experiments aimed to provide a proof-of-concept rather than demonstrating immediate use. Calibration curves were constructed for the ZnI emission line at 213.856 nm and the ZnII lines at 202.548 and 206.423 nm, and a LOD for environmental zinc was calculated. To ensure all observed signal originated from the zinc that had been incorporated into the bacterial cell, the suspension was washed three times as described in chapter three. After these washing steps, the suspension was centrifuged, and a sample of the supernatant was placed on a filter paper for testing. If zinc lines were observed in the filter spectrum, additional washing steps were used.

At environmental concentrations, the impact of additional zinc on bacterial spectra was immediately apparent, as seen in the spectra shown in Figure 7.4. While for the control plates, zinc lines were not readily distinguishable from noise, at 100 ppm, the lines became very noticeable. At all concentrations where zinc emission is resolvable, a

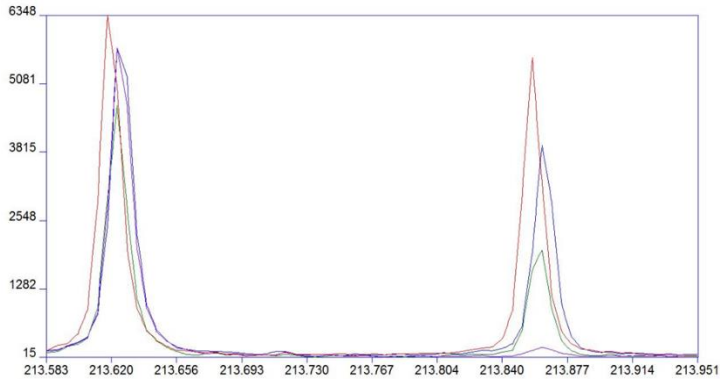

Figure 7.3: Zinc emissions at 213.856 nm from *E. coli* samples grown with excess zinc concentrations of 0 (purple), 100 (green), 200 (blue), and 300 ppm (red). To the left, a phosphorus emission line is shown for scale

fractional standard deviation in the measured intensity of approximately 25% was observed. This is in keeping with emission lines of comparable size from elements native to the bacterial cell. While all lines provided a strong linear correlation to environmental concentration, this correlation was strongest with the ZnI 213.856 nm emission line. The fit could be further improved with normalization of the measurement to the intensity of the neutral carbon 247.856 nm emission line as is shown in Figure 7.4. This normalization

Table 7.2: Correlation of emissions of observed zinc lines to concentration. The strongest correlation was observed with the 213.856 emission line, and correlation was uniformly improved with normalization to the 247.856 carbon line

	r^2	
Emission Wavelength (nm)	Raw Intensity	Normalized
202.548	0.882	0.977
206.423	0.883	0.981
213.856	0.983	0.994

was used to remove fluctuations in overall plasma intensity. This fit possessed an r^2 value of 0.994, and the fit was used to determine a limit of detection of 11 ppm zinc in the growth environment of the cells. The quality of fit for each emission line is shown in Table 7.2 for fits to both the raw emission intensity and that normalized to the emission on the

carbon line mentioned previously. WHO guidelines provide a limit of 5 ppm to zinc concentration of safe drinking water.[9]

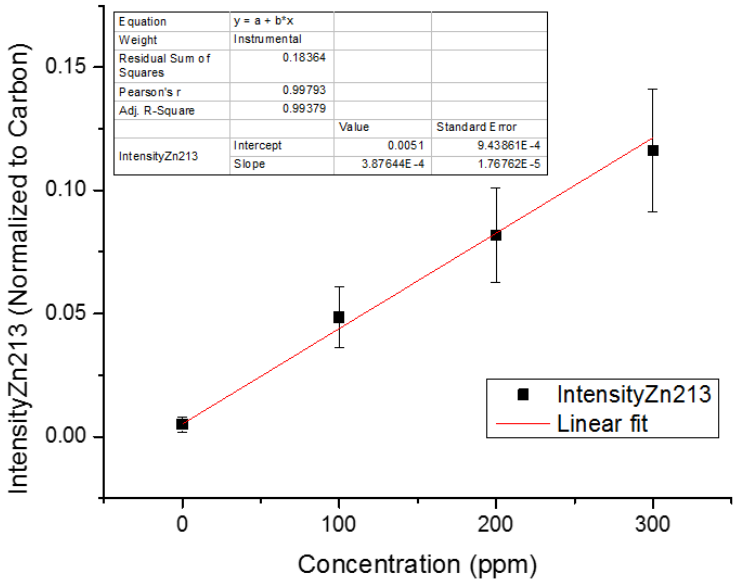

Figure 7.4: Measured LIBS emission of the zinc 213.856 nm line as a function of concentration. Emission intensity was normalized to the measured intensity of the carbon 247.856 nm emission line

7.3.2 Environmental Magnesium

Magnesium is a common contaminant in water. Compounds of magnesium along with those of calcium are the typical cause of hard water. Natural fresh-water concentrations of magnesium will generally range from 1 to over 100 ppm.[9] To investigate the impact of variations in environmental magnesium, *E. coli* was grown on agar plates doped with 200 and 300 ppm magnesium sulfate in addition to the magnesium already present in the growth medium. An attempt was made to precipitate magnesium from the growth medium via hydrochloric acid, but the resulting plates showed no growth.

For all concentrations of environmental magnesium, intensities of all six observed magnesium emission lines (emission observed at 279.078, 279.553, 279.800, and 280.270 nm for MgII, and 277.983 and 285.213 nm for MgI) were identical within the standard deviation of the measurements. This can be seen in Figure 7.5. However, samples grown in an excess of magnesium demonstrated a reduced deviation on magnesium lines. For all

lines except the larger 285.213 nm line of the neutral magnesium atom, the standard

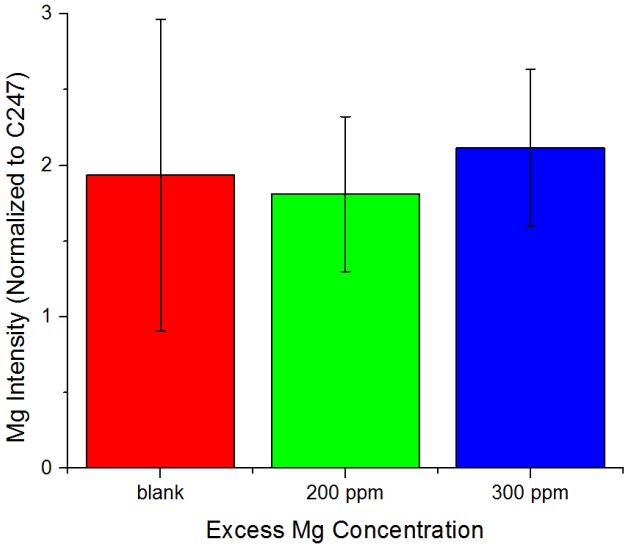

Figure 7.5: Magnesium intensity summed over all observed emission lines from bacteria grown in varied concentrations of excess magnesium. Emissions are normalized to carbon 257.856 nm emission intensity. While all emission intensities are equivalent within error, that of the samples grown in excess magnesium shows a considerably lower variation

deviation was reduced by more than half. The remaining line showed a reduction in variation by 40 and 45% for the 200 and 300 ppm concentrations respectively. While this suggests that a bacterial model for water hardness due to magnesium is not possible, it suggests that the active process of magnesium transport will maintain a constant magnesium concentration even in extreme environments. Experiments must be conducted to verify this result for other elements relevant to discrimination, but this gives the implication that bacterial classification will not be impacted by varied elemental concentrations in the growth environment.

It should be noted that this does not imply that the lines used for classification are inalterable by more chemically complex means. Since magnesium concentrations are maintained actively, it is likely possible to inhibit this mechanism through the use of certain compounds or proteins. This result shows only that the bacteria will not take up more magnesium from the environment than is needed by the cell.

References

[1] S.J. Rehse *et al.*, J. Appl. Phys., **105**, 102034 (2009)

[2] M. Baudelet *et al.*, Appl. Phys. Lett., **89**, 163903 (2006)

[3] L. Velásquez and J. Dussan, J. Hazardous Mat., **167** (1-3), 713 (2009)

[4] *Test ID: ZNS Zinc, Serum*, Mayo Medical Laboratories, <http://www.mayomedicallaboratories.com/test-catalog/Clinical+and+Interpretive/8620>

[5] *Reference ranges for blood tests*, Uppsala University Hospital (2008)

[6] *F. Veglio and F. Beolchini,* Hydrometallurgy, **44**, 301 (1997)

[7] J.B. Fein *et al.*, Geochim. Cosmochim. Acta, **61** (16), 3319 (1997)

[8] *Water Hardness, United States School of Geological Survey School of Water Science <http://water.usgs.gov/edu/hardness.html> (2016)*

[9] D. Chapman, *Water Quality Assessments- A Guide to Use of Biota Sediments and Water in Environmental Monitoring*, 2nd Ed. (Cambridge, England, 1996) pp. .

[10] *CCME Summary Table*, Canadian Council of Ministers of the Environment <http://st-ts.ccme.ca/en/index.html?chems=229&chapters=1,2,3,4,5> (1999)

[11] P. Dimroth, Philos. Trans. R. Soc. Lond. B Biol. Sci., **326** (1236), 465 (1990)

[12] M.B. Moncrief and M.E. Maguire, J. Biol. Inorg. Chem., **4** (5), 523 (1999)

[13] H. Lodish *et al*, *Molecular Cell Biology*, 4th Ed. (New York, USA, 2000) <http://www.ncbi.nlm.nih.gov/books/NBK21481/>

[14] *Normal and Diabetic Blood Sugar Level Ranges*, Diabetes UK <http://www.diabetes.co.uk/diabetes_care/blood-sugar-level-ranges.html> (2016)

Chapter 8: Spectra of Inactivated and Sterilized Bacteria[ii]

8.1 Motivation

LIBS for the identification of bacteria has been pursued as a means of diagnosis in the medical field. As is implied by the task, this creates a certain level of risk due to the handling of bacterial specimens. Because many methods of bacterial identification rely on cell reproduction, many current techniques require these pathogenic specimens be alive, and as such, dangerous. LIBS is an elemental assay that provides purely compositional information. If a bacterial specimen is rendered inert via methods that do not require the addition of chemical compounds, LIBS should not be expected to provide information on the metabolic state of bacteria. This hypothesis is still disputed in the literature. Spectra from live, heat-killed, and UV-inactivated bacteria were shown to be indistinguishable via DFA by Mohaidat et al. in 2011.[1] However, Multari et al. published a contradictory result for discrimination of heat-killed bacteria in 2013 using a similar 1064 nm nanosecond laser system.[2] In 2015, Sivakumar presented similar results for *E. coli* treated via heat-killing and sonication using a femtosecond-pulse laser for ablation, but reported inconclusive results when using laser pulses of nanosecond duration.[3] My intent with these studies is to provide an updated result to Mohaidat's initial experiment using our new mounting procedure. If bacteria that have been killed by exposure to heat or ultraviolet light are differentiable from living cells, it then becomes important to determine if discrimination of species is still possible with a library of sterile cells.

8.2 Methods of Bacterial Inactivation and Sterilization

Three methods of "killing" bacteria are typically discussed in bacterial LIBS literature: sonication, UV exposure, and heat-killing via autoclave.[1-4] Sonication is the use of high-intensity ultrasonic pulses to mechanically disrupt the cellular membrane of the bacteria resulting in lysis. This method was not used for our experiments but is worth noting due to its use in similar studies.

[ii] These experiments were the result of collaboration with D.J. Gillies and were published earlier this year.[4]

Sterilization via autoclave is regarded as one of the most dependable methods for sterilization of pathogens by the Centre for Disease Control.[5] Autoclaves saturate a pressurized atmosphere with steam, generally at a temperature of 121°C. There are two standard types of autoclave: gravity displacement and high-speed prevacuum autoclaves. A gravity displacement autoclave, as that used in these experiments, has samples placed in a sealed environment while steam is pumped into the chamber from the top or walls. The steam forces the air in the chamber out through vents in the floor, and the sample is left for a proscribed amount of time depending on the size and nature of the sample for sterilization. For these experiments, samples were autoclaved in suspension for 40 minutes. This system is best for a non-porous sample to which the steam has easy access. The high-speed prevacuum autoclave uses a vacuum pump to remove air from the autoclave chamber prior to the addition of steam. This ensures that the steam can penetrate the entire sample.[5, 6]

Exposure of bacteria to bactericidal ultraviolet rays is a method of bacterial inactivation. This differs from sterilization in that it does not, strictly speaking, kill the exposed cells. The previously discussed methods for sterilization irreparably damage the cells such that they can no longer function. Exposure to UV light in the range of 200-280 nm causes genetic damage to the cells in the form of the creation of pyrimidine dimers, typically in sequential thymine bases.[6, 7] Ultraviolet photons are absorbed by the double bonds in the nucleotide's carbon ring, breaking it. This then results in bond formation between the two adjacent bases. An example of this molecular genetic damage is given in

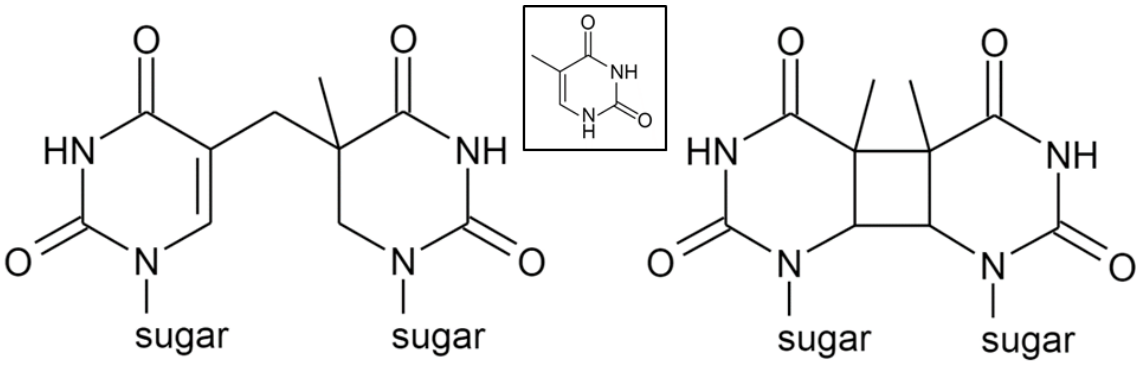

Figure 8.1: Two potential thymine photodimers produced via irradiation with UV light. The initial structure of thymine is shown in the insert for comparison

figure 8.1.[7] This damage inhibits DNA replication, preventing cell division. While this method is useful for surface decontamination, the low penetrative power of UV photons limits its efficacy and this is not a preferred method for complete sterilization.[6]

8.3 Classification of "Killed" Bacteria with Live Groups

8.3.1 Autoclaved *E. coli*

Samples of *E. coli* were autoclaved in suspension in distilled water. This suspension was then used to streak an agar plate and allowed to incubate for 48 hours to verify sterility. 35 spectra were acquired from a filter prepared in the usual method. No changes in the spectra were immediately apparent. The variation of spectral lines was found to be comparable to live samples, and total unnormalized intensities for the lines of interest were identical to those from untreated samples within error. These spectra were classified using discriminant function analysis and the data library described in chapter four. Spectra were classified near uniformly as *E. coli* with one file being misclassified as *P. aeruginosa*. However, it is visible when the data is plotted by its first and second discriminant scores as in Figure 8.2 that there is in fact a systematic shift in the data. The autoclaved spectra

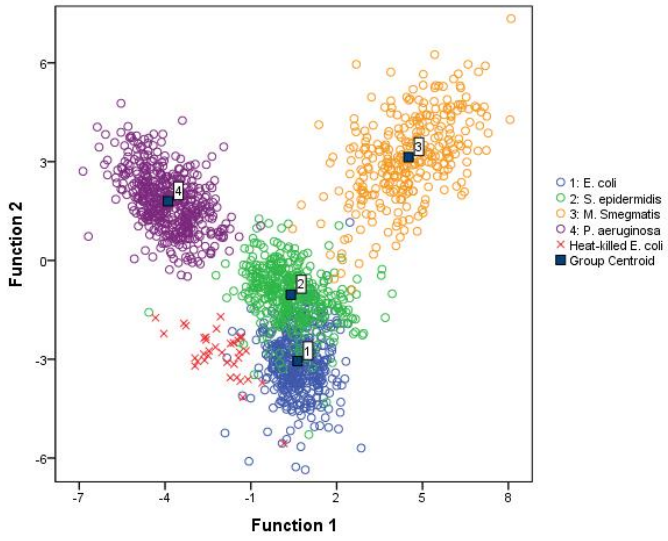

Figure 8.2: Plot of the first two discriminant scores for the four library species as well as heat-killed *E. coli* (red x's). While nearly all heat-killed samples classify as *E. coli*, a systematic shift is observable in the first discriminant score

do not overlap with the spectra from live bacteria. This suggests that while autoclaved *E.*

coli more closely resembles live *E. coli* than any other species in our current library, there is a marked change in the spectra observed from the two groups.

It has been proposed by Sivakumar that spectral shifts in autoclaved bacteria may be due to a lysis of autoclaved cells and a resulting loss of intracellular material prior to ablation.[3] While this is possible, SEM images of a bacterial lawn formed from autoclaved

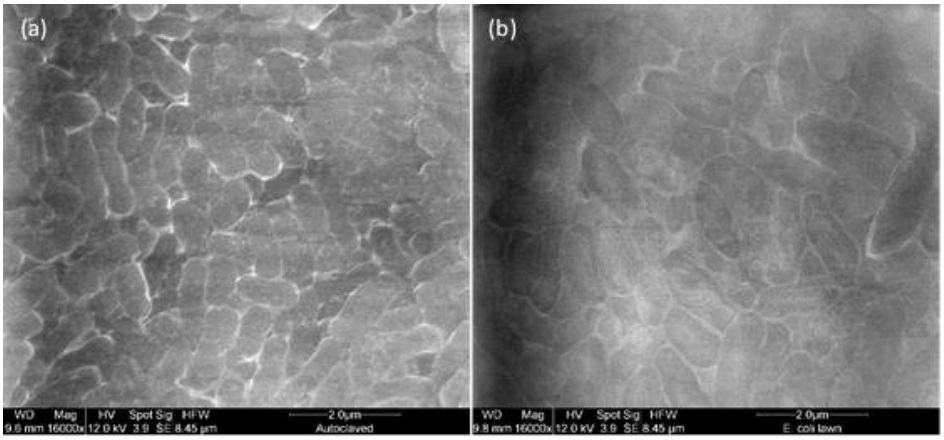

Figure 8.3: SEM images acquire of (a) autoclaved and (b) live *E. coli*. Differences in contrast are artifacts of the imaging process and do not show changes between samples

cells show no visible difference from live specimens (Figure 8.3). This has led to two questions that must be addressed. If lysis is the cause of the spectral change, then a method of cellular inactivation that is non-destructive should not result in any alteration to the discriminant score for those spectra. The loss of intracellular material is also not likely to have a uniform effect on all species of bacteria. As such, it may not be possible to classify autoclaved bacterial samples using the existing library. For this reason, a library of bacterial spectra was collected from autoclaved samples in order to ensure that a classification of autoclaved samples is possible.

8.3.2 UV Inactivated *E. coli*

Inactivated *E. coli* samples were prepared by following the usual methods for sample preparation. Once the bacterial lawn was formed on the filter paper, the filters were placed under a 4 W bactericidal UV lamp emitting at 254 nm (UVG-11 Compact UV Lamp, UVP, LLC). Three filters were used for data acquisition with exposure times of 15, 45, and 60 minutes resulting in 35, 49, and 34 spectra respectively. Additional filters were prepared as above, but these filters were then pressed against the surface of agar plates

to check for growth. After 48 hours, no regrowth was observed for any exposure time. Each filter was classified against the library discussed in chapter 4. All of the 118 files were classified as *E. coli* by the discriminant function analysis. Again, however, a shift in the discriminant score for these data files was observed. It can be seen in the plot of the first

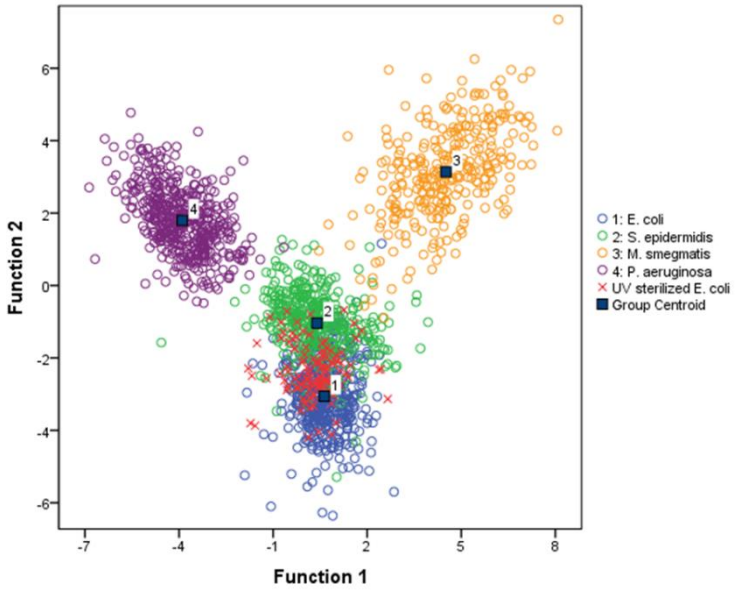

Figure 8.4: Plot of discriminant scores for four species as well as UV sterilized *E. coli* (red). While all 118 spectra were classified with the proper species, a shift in discriminant score 2 is apparent. This shift is less dramatic than that observed in heat-killed specimens and is in a score that holds less weight in classification, indicating that the change in emissions is more subtle or affects atomic species less relevant to classification

two discriminant scores (Figure 8.4) that the "centre of mass" of these scores was shifted to higher values of the second discriminant score. This result implies a separation of the groups that is not substantial enough to confuse the discrimination but does exist nonetheless.

8.3.3 Discrimination of Metabolic States

In order to state whether these groups were significantly different, a discriminant function analysis was performed with three groups: live, UV inactivated, and autoclaved *E. coli*. This analysis generated two discriminant functions, and the scores of the groups can be seen in Figure 8.5 below. To determine whether membership to these groups was

truly discernable, the Wilk's lambda for these functions was calculated. The Wilk's lambda is an inverse measure of quality defined as

$$\Lambda = \sum \frac{1}{1+\lambda} = \frac{\text{unexplained variance}}{\text{total variance}}$$

where λ is the eigenvalue of a given discriminant function and the sum is over some number of eigenvalues.[8] The result is a value between 0 and 1. This was provided in the

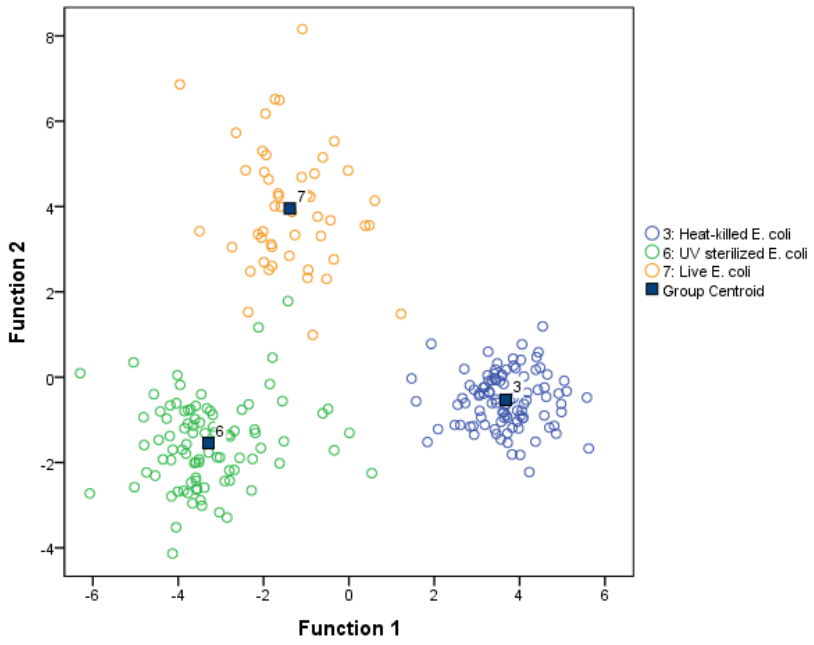

Figure 8.5: Plot of discriminant scores for *E. coli* samples of various metabolic states

output of our analysis software as the lambda of all functions, then that of the second through last, then third through last, and so on. This, in essence, provides the discriminating power of the analysis as a whole in the first value, then removes the score of most importance before retesting.

When performing an analysis of our three metabolic states, heat-killed, viable, and UV inactivated, a Wilk's lambda of 0.017 was achieved in the full discrimination, while the second discriminant score yielded a value of 0.190. For comparison, in discriminating between four genera of bacteria, Wilk's lambdas of 0.004, 0.036, and 0.242 were obtained. A low value in this test indicates that the discriminant scores obtained from the spectra of these bacteria account for a large portion of the observed fluctuation. Based on the above result, a DFA can account for 98.3% of the variation in the data. This leads

us to conclude that there are discernable differences in the spectra of these three metabolic states within a single bacterial species.

It is important to note that, in the context of the discrimination between the four genera that has been discussed, these difference are not of note. That is to say, these differences do not interfere with the classification of the bacteria between species and are only noticeable when they were directly investigated. For clinical purposes, these bacteria classify with their species. This suggests that a sample of unknown metabolic state would not be an impediment to this method of identification.

8.4 Classification of Four Species After Heat-Killing

A library of spectra from heat-killed bacteria was constructed as a proof-of-concept. The current hypothesis in the LIBS community regarding the shift in spectra related to heat-killing is a potential loss of intracellular material via lysis of the cells.[3] While the majority of the metals important to classification using LIBS are located in the cellular envelope, this loss of materials is likely inconsistent between species. For this reason, a library of spectra was collected from autoclaved bacteria to ensure that a classification could be performed entirely with heat-killed samples.[9] This would guarantee a far safer environment for those working in pathology labs as all samples could be sterilized before handling.

For each species, 100 bacterial spectra were acquired. DFA was performed using both RM2 and RM3. The initial analysis was performed with RM2 because this model included far fewer variables than RM3 which was expected to prevent over-defining the data with so few spectra. External validation was repeated with RM3 to determine the extent to which such an over-definition would alter results.

The plot of the first two discriminant scores for this classification is shown in Figure 8.6. This plot was generated during an external validation to test the sensitivity and specificity of the library. 20 files from the library were withheld from the DFA for the generation of the discriminant functions. These files were then classified using the functions generated in their absence. Upon inspection, it is clear that discrimination for all species aside from *P. aeruginosa* has become more difficult. The first discriminant score

accounted for 48.8% of the observed variance in the discrimination of live species. When performing the same analysis with heat-killed bacteria, the first score accounted for 87.0% of variance, but only separated one species out clearly. Despite this, the accuracy of the

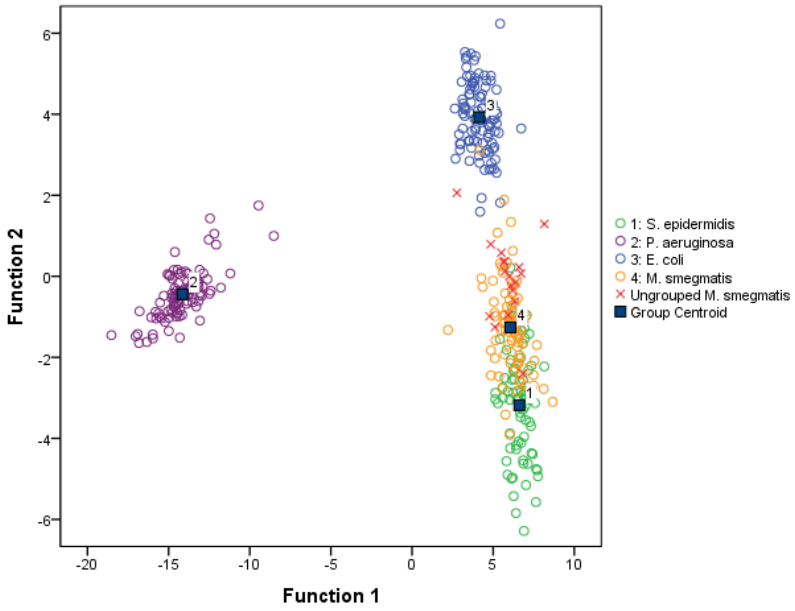

Figure 8.6: Plot of discriminant scores for a library of heat-killed bacteria. This plot was generated during external validation with 20 *M. smegmatis* spectra withheld for classification

classification did not greatly suffer. A sensitivity of 96 ± 4% was observed with a specificity of 99 ± 3%. When repeating this analysis with RM3, results were identical for sensitivity, and the specificity was marginally improved. This improvement came in the form of a reduction in the error of the sensitivity, dropping from 4% to 2%, and a negligible increase in specificity, from 98.65% to 98.68%. The addition of variables between the two models did not seem to result in any over-definition of these data.

As was observed in chapter 4, LIBS can provide classification of bacteria from four genera with near-perfect accuracy. When the bacteria are treated via autoclave, this classification suffers, but the change is only minimal. It is also worthy of note that classification accuracy has been observed to increase with the addition of spectra to the model, and the sterile library was a fourth the size of that discussed previously. This result shows that not only might LIBS be a fast and reliable tool for diagnosis of bacterial infections, but it could also provide a far safer laboratory environment for such tests.

References

[1] Q. Mohaidat, S. Palchaudhuri, S.J. Rehse, Appl. Spectrosc., **65** (4), 386 (2011)

[2] R.A. Multari *et al.*, J. Agri. Food Chem., **61**, 8687 (2013)

[3] P. Sivakumar *et al.*, Astrobiol., **15** (2), 144 (2015)

[4] D.J. Malenfant, D.J. Gillies, and S.J. Rehse, Appl. Spectrosc., **70** (3), 485 (2016)

[5] *Guideline for Disinfection and Sterilization in Healthcare Facilities*, Centers for Disease Control and Prevention <http://www.cdc.gov/hicpac/disinfection_sterilization/13_0sterilization.html> (2008)

[6] S. Rao, *Testing of disinfectants*, <http://www.microrao.com/micronotes/pg/testing_of_disinfectants.pdf>

[7] D.S. Goodsell, Oncologist, **6** (3), 298 (2001)

[8] D.G. Assimakopolus *et al.*, *Knowledge Perspectives of New Product Development: A Comparative Approach*, 1st Ed. (Berlin, Germany, 2011)

[9] S.J. Rehse *et al.*, J. Appl. Phys., **105**, 102034 (2009)

Chapter 9: Conclusions and Future Work

9.1 Conclusions

The aim of this work was to showcase the robustness of laser-induced breakdown spectroscopy as a tool for clinical microbiologists and diagnosticians. Experiments regarding the mounting of live bacterial samples on nitrocellulose filter paper rather than on background-free media or as freeze-dried pellets showed that reproducible spectra could be acquired in spite of the strong carbon emissions observed as a result of the filter. A library of these spectra were acquired, and it was shown that typical chemometric techniques for classification could distinguish bacteria at the genus level with near-perfect accuracy. The use of both discriminant function analysis (DFA) and partial least-squares discriminant analysis (PLS-DA) were investigated. These techniques were shown to provide identical results. Analysis through external validation provided a rate of true positives (sensitivity) of 98 ± 2% and a rate of true negatives (specificity) of 99 ± 1% when using DFA. When employing PLS-DA, a sensitivity and specificity of 97 ± 3% and 99 ± 2% were achieved.

Studies were conducted into the impact that the titer of the bacterial suspension has on LIBS signal intensity. A calibration curve was constructed across two orders of magnitude of dilution. It was found that suspensions used for the construction of a classification library were in the saturation regime for LIBS response. A strong linear trend was found between the sum of the integrated intensity of atomic emission lines used for classification and the titer of the bacterial solution for titers less than 10^9 CFU per mL. Such a suspension would generate a bacterial lawn where 10^5 CFU would be ablated by each laser pulse. However, as signal intensity decreased, fractional variation in the intensity became unacceptably large. A limit of detection was calculated at 48000 ± 12000 CFU per ablation event. Since typical retrieval rates for a nasal swab are on the order of hundreds of colony forming units, this limit is very unrealistic.[1]

In an attempt to reduce the number of colony forming units required for detection, an insert was designed for centrifuge filtration. The device was designed such that a filter could be placed in it before the addition of up to 1.5 µL of suspension. The device was

then inserted into a centrifuge tube, and centrifuged at 2500 rpm for three minutes. It was believed that by causing the bacteria to settle into a lawn faster, clumping of cells could be minimized, resulting in a more reliable signal at low cell counts. Again, a calibration curve was constructed. While the plasma emission intensity measured from samples prepared in this method was far more reproducible, the limit of detection was increased to 90000 ± 9000 CFU per ablation event. While this method did not improve the limit of detection, it did provide a much more rapid means of mounting bacteria obtained from low titer specimens while improving signal reliability.

Emissions from bacteria grown on agar plates doped with excesses of biologically relevant elements and molecules were investigated. Magnesium, zinc, and glucose were chosen as representative dopants. Zinc and magnesium are both metals, but one of them (magnesium) is very relevant to bacterial classification and the other (zinc) is not typically observed in our bacterial plasmas at all. The molecule glucose was chosen because it was believed that it would provide an excess metabolic energy source for active transport of metals. When doped into the agar at the concentrations one finds in the human body, neither zinc nor magnesium caused any observable effects in the bacterial plasma. *E. coli* was grown on agar with glucose concentrations representative of blood glucose for individuals with type 1 and children's type 1 diabetes as well as that of a healthy individual. Spectra from bacteria grown on these plates were classified as *E. coli* with a true positive rate consistent with the accuracy of the library used for discrimination. When bacteria were grown on agar with excess metal concentrations consistent with environmental contamination, it was found that magnesium uptake appears to be actively regulated such that no alteration to intensity was observed. Conversely, the intensity of zinc emissions at the 202.548, 206.423, and 213.856 nm transitions were found to strongly correlate with environmental zinc concentration. This correlation was improved with normalization to emissions from carbon at 247.856 nm. A limit of detection of environmental zinc based on LIBS performed on *E. coli* was determined to be 11 ppm. This is of the appropriate order of magnitude to detect contamination in drinking water.[2]

The effect of the cells' metabolic state on bacterial classification was investigated to determine if sterilization of samples prior to testing was possible. This would create a much safer environment for clinicians, as all bacteria-containing specimens could be reduced to biosafety level one (BSL1) before handling. Both heat-killing and UV sterilization were shown to have a noticeable and reproducible impact on the discriminant scores of bacteria. This effect was not enough to interfere with classification in a meaningful way. It was shown through DFA that these three metabolic states are discernably different. As a counter to the systematic shift in discriminant scores of bacteria treated by autoclave, a library of heat-killed bacteria was assembled. This library showed a shift in the locations of the group centroids for each species in discriminant score space when compared to the library of spectra acquired from live samples, but this does not appear to have an impact on discrimination. A sensitivity and specificity of 96 ± 4% and 99 ± 2% were achieved for this library.

These results indicate that I have indeed demonstrated a new mounting procedure that provides a reproducible bacterial LIBS signal without interfering with classification using tools familiar to clinicians and diagnosticians. These results also illustrate the robustness of LIBS measurements on samples grown in biological conditions and show that LIBS can provide a method of bacterial identification that reduces the risk of infection to clinical microbiologists compared to what is presently available.

9.2 Future Work

The largest hurdle LIBS must overcome before it can be used as a diagnostic tool is that of cell count. A limit of detection must be achieved that is comparable to the number of colony forming units retrieved in a clinical sample. Presently, the obstacle for this work comes in the form of emissions from the nitrocellulose filter paper. This results in a persistent line at 247.856 nm that limits the amplification of the spectrometer that can be used without causing damage to the ICCD chip. The integration of a notch filter to the collection optics would limit this issue. Those offered by Thorlabs, Inc provide over a 90% transmittance at wavelengths outside of the range of the band-stop with an optical density of at least 6 (giving a reduction in intensity by a factor of 10^6) inside that range.

This filter, however, would need to be custom-constructed for this wavelength, making it a costly solution to implement. Many groups employ multiple high-resolution spectrometers that cover small bandwidths in order to construct their LIBS spectra. It would be possible to construct an apparatus that uses two spectrometers that measure emissions above and below the carbon line, but this solution is considerably more costly than the use of a notch filter. Once the necessary cell count per ablation event is achieved, it would require only a simple modification to the centrifuge filtration insert to force all the bacteria in a sample to filter through the same 150 micron diameter location on the filter paper. This would allow for a single ablation with a sufficient number of cells so long as a fluid sample with that many cells could be acquired, regardless of the titer of that suspension.

It has been proposed on multiple occasions that the sensitivity of LIBS could be improved by integrating the spectral data achieved from laser ablation with molecular information provided by Raman spectroscopy. This technique measure shifts in frequency of laser light incident on a sample caused by Stokes and anti-Stokes scattering. This occurs when a photon incident on a material has energy absorbed (Stokes) or when the material loses energy to the photon (anti-Stokes) during an inelastic scattering event. These changes in energy correspond to changes in vibrational modes for the molecule of interest.[3] While it has been shown that LIBS has great potential for discrimination alone, the addition of structural information that can be provided with Raman spectroscopy to the compositional data generated by LIBS may be able to create a far more robust bacterial fingerprint.

It was shown in this work that bacteria will take up environmental zinc during their growth. However, the location of this zinc is not known. Experiments can be conducted to determine whether zinc is integrated or attached to the cellular membrane of bacteria or if it is taken into the cytoplasm. These experiments could be conducted using a similar procedure to Rehse's work in 2009, wherein the bacterial membranes were isolated for LIBS. If measured emissions show a considerable decrease after cell lysis, then it can be assumed that the metal is making its way into the cytoplasm.[4] In a similar vein, tests could

be conducted to determine if zinc uptake is an active process in the cell or if it is passively transported through the membrane. To investigate this, two samples should be prepared in a liquid medium doped with zinc sulfate, one live and the other heat-killed. After some amount of time, each sample can be interrogated via LIBS and their zinc emissions compared. In its simplest outcome, that is, not accounting for the unexpected, one of three results should be obtained: live bacteria show a higher zinc emission than those that were heat-killed, indicating that zinc transport is an active process; the two samples show similar emission intensities, indicating a passive transport mechanism; or heat-killed bacteria show higher emissions from zinc. This final result could suggest that zinc is actively rejected by the cell, but more slowly than it is taken in. This would begin to demonstrate the potential utility of LIBS to biological studies outside the problem of classification.

Continued efforts in the field push LIBS closer to becoming a useful diagnostic resource. These results have been a contribution to that effort. However, much more work is still necessary to make that a reality. Time should also be dedicated to explorations of the potential utility of LIBS for biological research. Classification and detection, while the fundamental goal of LIBS on bacteria, are only one of many possible applications of this technology.

References

[1] P. Warnke *et al.*, PLoS ONE, **9** (10), e111627 (2014)

[2] D. Chapman, *Water Quality Assessments- A Guide to Use of Biota Sediments and Water in Environmental Monitoring*, 2nd Ed. (Cambridge, England, 1996) pp. .

[3] E.V. Efremov, F. Arisee, and C. Gooijer, Analytica Chim. Acta, **606**, 119 (2008)

[4] S.J. Rehse *et al.*, J. Appl. Phys., **105**, 102034 (2009)

Vita Auctoris

NAME: Dylan J. Malenfant

YEAR OF BIRTH: 1991

EDUCATION: B.Sc. [Honours] Medical Physics, 2014
University of Windsor, Windsor, On

M.Sc. Physics, 2016
University of Windsor, Windsor, On